Journal of Medicinal Chemistry

Article

Cite This: J. Med. Chem. 2018, 61, 6904−6917

pubs.acs.org/jmc

Unraveling the Prenylation−Cancer Paradox in Multiple Myeloma with Novel Geranylgeranyl Pyrophosphate Synthase (GGPPS) Inhibitors

Cyrus M. Lacbay,[†,⊥] Daniel D. Waller,[‡,⊥] Jaeok Park,[§] Mònica Gómez Palou,[‡,⊥] Félix Vincent,[†] Xian Fang Huang,[‡] Viviane Ta,[†] Albert M. Berghuis,[§] Michael Sebag,*[,‡,∥] and Youla S. Tsantrizos*[,†,§]

[†]Department of Chemistry, McGill University, Montreal, QC H3A 0B8, Canada

[‡]Department of Medicine, McGill University, Montreal, QC H3A 1A1, Canada

[§]Department of Biochemistry, McGill University, Montreal, QC H3G 1Y6, Canada

[∥]Division of Hematology, McGill University Health Center, Montreal, QC H4A 3J1, Canada

Supporting Information

ABSTRACT: Post-translational prenylation of the small GTP-binding proteins (GTPases) is vital to a plethora of biological processes, including cellular proliferation. We have identified a new class of thienopyrimidine-based bisphosphonate (ThP-BP) inhibitors of the human geranylgeranyl pyrophosphate synthase (hGGPPS) that block protein prenylation in multiple myeloma (MM) cells leading to cellular apoptosis. These inhibitors are also effective in blocking the proliferation of other types of cancer cells. We confirmed intracellular target engagement, demonstrated the mechanism of action leading to apoptosis, and determined a direct correlation between apoptosis and intracellular inhibition of hGGPPS. Administration of a ThP-BP inhibitor to a MM mouse model confirmed in vivo down-regulation of Rap1A geranylgeranylation and reduction of monoclonal immunoglobulins (M-protein, a biomarker of disease burden) in the serum. These results provide the first proof-of-principle that hGGPPS is a valuable therapeutic target in oncology and more specifically for the treatment of multiple myeloma.

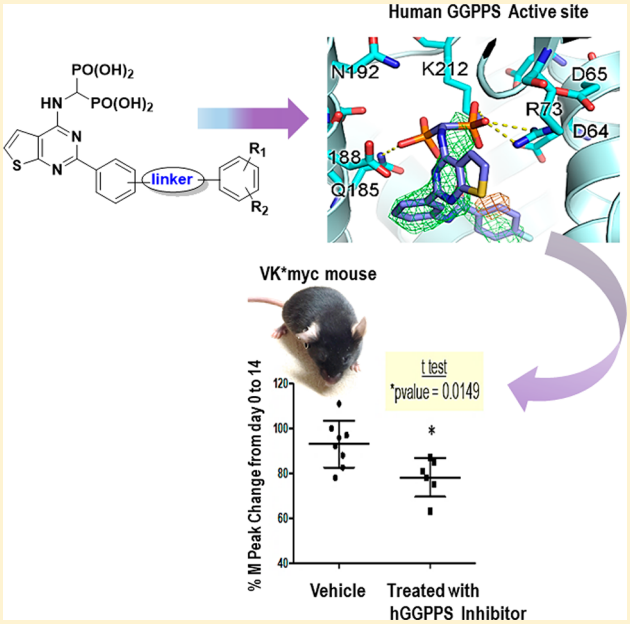

INTRODUCTION

Post-translationally modified proteins, with either farnesyl pyrophosphate (FPP) or geranylgeranyl pyrophosphate (GGPP), constitute approximately 2% of the total mammalian proteome.[1] Known farnesylated proteins include members of the small GTP-binding proteins (GTPases), such as the Ras superfamily (e.g., H/K/N-Ras),[2] DnaJ chaperone proteins,[3,4] and the precursor of the nuclear lamin A.[5] Geranylgeranylated GTPases include the Rho family of proteins (e.g., RhoA/B/C), the Ras-related proteins Rap1A and Rac-1, and Cdc42. Prenylation of small GTPases provides them with the ability to associate specifically with cellular membranes and participate in a plethora of cellular functions, including cell signaling and proliferation.[6]

There is a growing awareness that dysregulation of the mevalonate pathway plays a crucial role in oncogenesis and tumor cell survival.[7−9] In the past, targeting this pathway has focused mainly on inhibiting the human farnesyl pyrophosphate synthase (hFPPS) and the prenyl transferases FTase and GGTase I (Figure 1a). Indirect inhibition of prenylation with statins[10−12] has also been under clinical investigation and implicated in better survival of patients with multiple myeloma (MM).[13] Nitrogen-containing bisphosphonates (*N*-BPs; Figure 1b), such as zoledronic acid (**1**; ZOL) and risedronic acid (**2**; RIS), are clinically validated inhibitors of hFPPS that are used mainly for the treatment of skeletal disorders.[14,15] Additionally, the potential value of *N*-BPs as antitumor agents has been explored in numerous studies both in vitro and in vivo. For example, clinical trials in breast cancer[16−19] and MM[20,21] have shown improved outcomes for patients treated with standard of care chemotherapy plus zoledronic acid (**1**)

Received: June 4, 2018
Published: July 17, 2018

DOI: 10.1021/acs.jmedchem.8b00886
J. Med. Chem. 2018, 61, 6904−6917

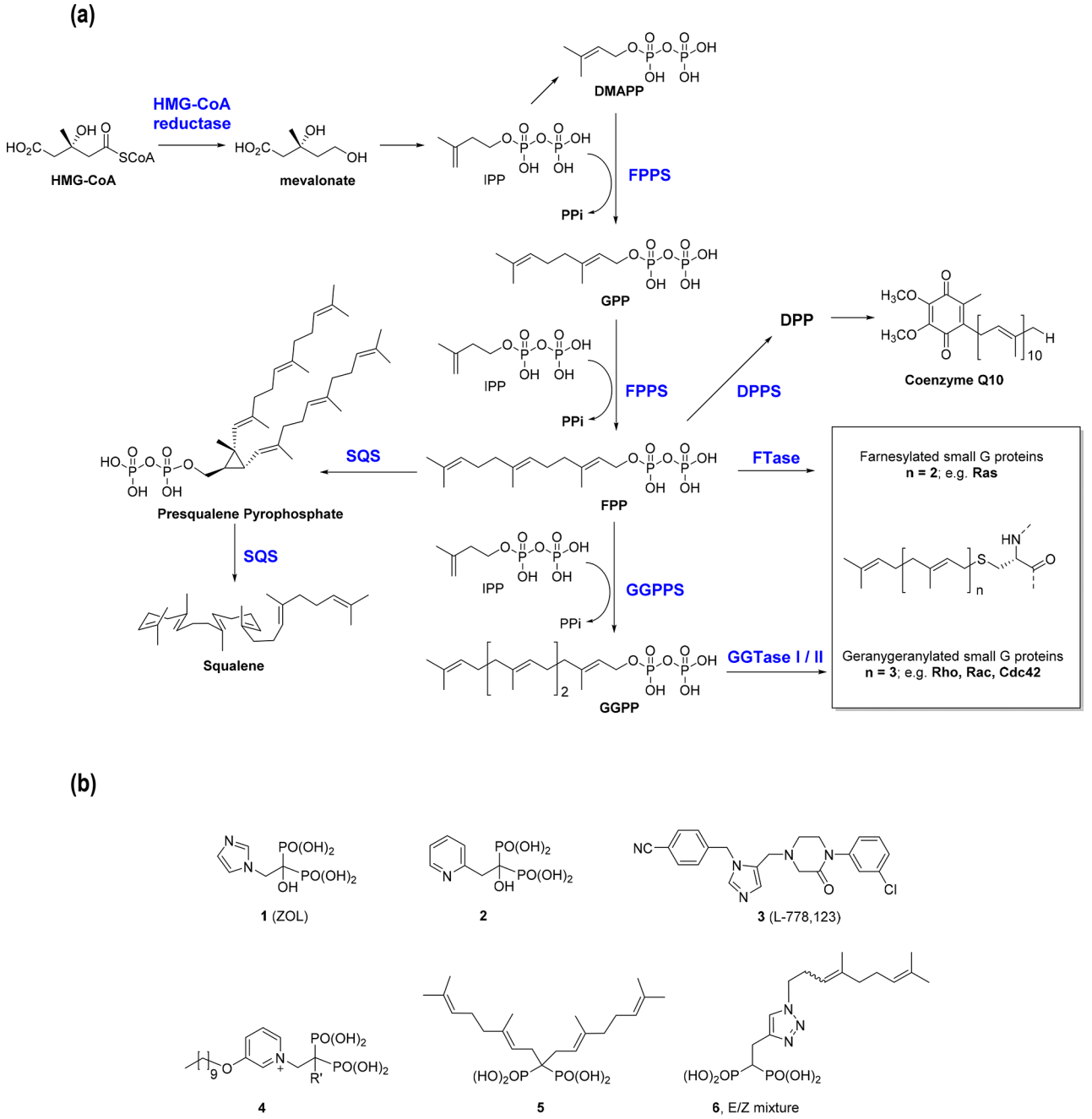

Figure 1. Isoprenoid substrates and inhibitors of prenylation. (a) Sequence of biochemical steps involved in the biosynthesis of isoprenoids. (b) Structures of inhibitors zoledronic acid (**1**) and risedronic acid (**2**) of hFPPS. L-778,123 (**3**) is a dual inhibitor of FTase and GGTase I. Compound **4** is a dual inhibitor of hFPPS and hGGPPS. Compounds **5** and **6** are selective inhibitors of hGGPPS.

and the effects appeared to be unrelated to the skeletal benefits of this drug. However, there is an ongoing debate as to whether *N*-BPs are bona fide antitumor agents, since their antitumor effects in humans are minimal when used in monotherapy. The modest clinical antitumoral efficacy of **1** has been attributed to its poor cell-membrane permeability, rapid clearance from the systemic circulation, and almost negligible distribution to nonskeletal tissues.[22,23] Consequently, more recent drug discovery efforts have focused toward the identification of non-bisphosphonate allosteric inhibitors of hFPPS.[24−27] Numerous structurally diverse compounds have been reported; unfortunately, none of them exhibit any significant antitumor potency. Efforts directed at blocking the prenyl transferase enzymes FTase and GGTase I have also received significant attention. Several compounds, including the dual FTase/GGTase I inhibitors L-778,123 (**3**),[28,29] were advanced to clinical development. However, after a number of disappointing clinical trials with FTase inhibitors, it was realized that a biochemical redundancy mechanism allows cross prenylation and activation of Ras proteins (which are common drivers of oncogenesis) by GGTPase I, when FTase is inhibited.[30,31]

The human geranylgeranyl pyrophosphate synthase (hGGPPS) is not yet a clinically validated therapeutic target. Only a few selective inhibitors of this enzyme have been reported, and none advanced to clinical development. The

DOI: 10.1021/acs.jmedchem.8b00886
J. Med. Chem. 2018, 61, 6904−6917

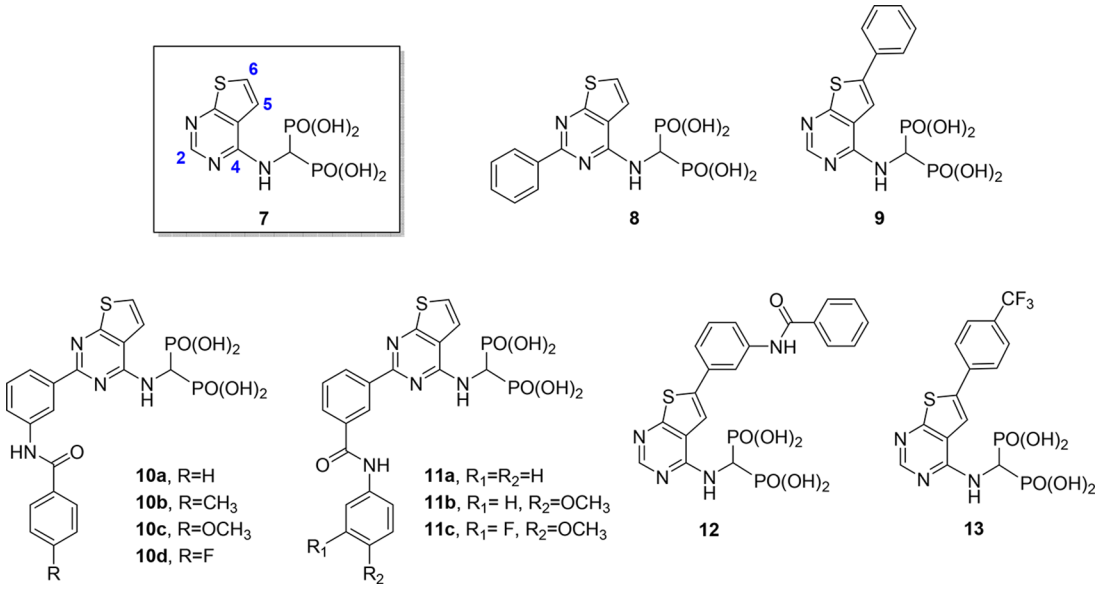

Figure 2. Examples of thienopyrimidine-based inhibitors of hFPPS/hGGPPS.

Scheme 1. Parallel Synthesis of a 60-Member Compound Library[a]

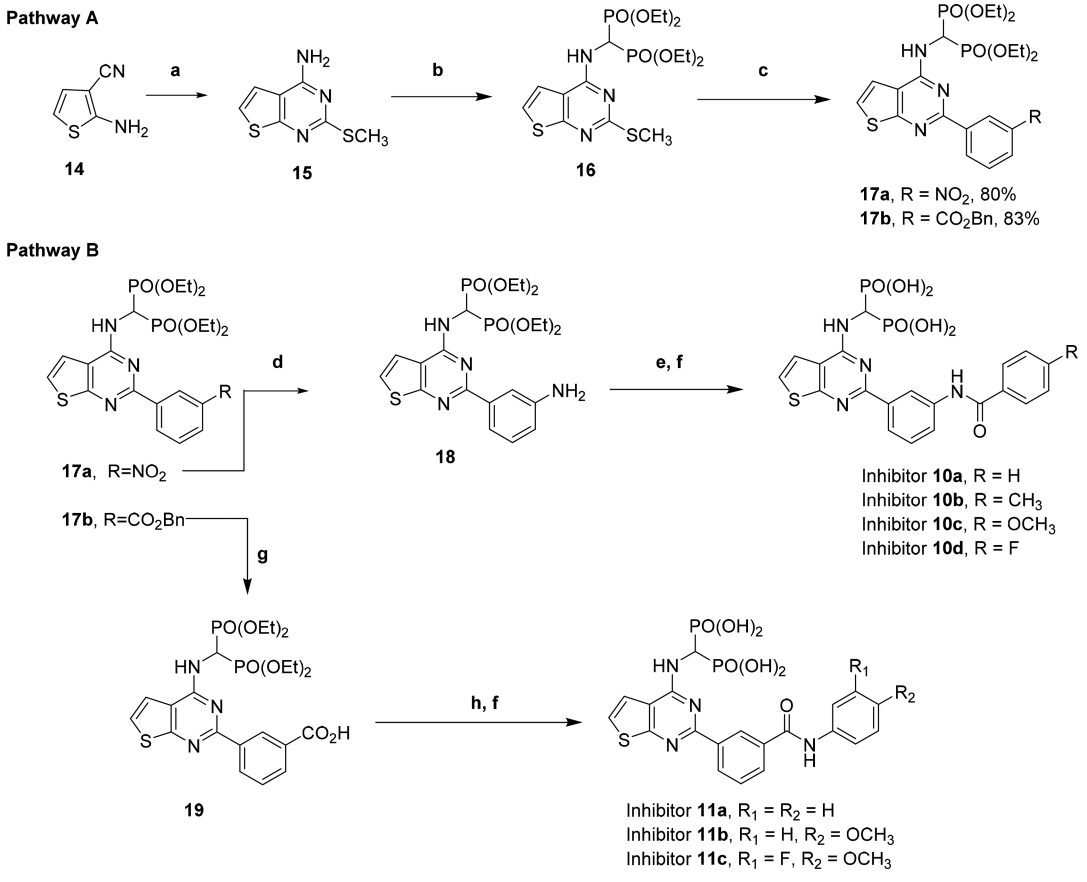

[a]Pathway A: Synthesis of key intermediates **17a,b**. Pathway B: Synthesis of compound library, including analogs **10a−d** and **11a−c**. Conditions: (a) MeSCN, HCl, dioxane, 70 °C, 63%; (b) diethyl phosphite, $CH(OEt)_3$, toluene, 130 °C, 40%; (c) arylboronic acid, $Pd(dppf)Cl_2{\cdot}CH_2Cl_2$, CuTC, dioxane, 50 °C, 80−83%; (d) $SnCl_2{\cdot}H_2O$, EtOH, 80 °C, 83%; (e) aryl/heteroaryl acid chloride, Et_3N, DCM, 0 °C to rt or aryl/heteroaryl carboxylic acid, HBTU, DIPEA, DMF, rt, 60−80%; (f) TMSBr, DCM, 0 °C to rt, then MeOH; (g) TFA, 80 °C; >95%; (h) H_2N-aryl/heteroaryl, HBTU, DIPEA, DMF, rt, 60−80%.

precision with which hGGPPS identifies its substrates surpasses our current understanding of the molecular recognition elements required to design potent and highly selective inhibitors for this target. Although the volume of the hGGPPS active site cavity is larger than that of its functionally related upstream enzyme, hFPPS, this information alone does

DOI: 10.1021/acs.jmedchem.8b00886
J. Med. Chem. 2018, 61, 6904−6917

not provide sufficient guidance in the design of selective and drug-like inhibitors. Known inhibitors of hGGPPS include the pyridinium bisphosphonate **4**[32,33] and the substrate bioisosteres **5**[34] and **6**[35] (Figure 1b). Compound **4** exhibits negligible selectivity between hFPPS and hGGPPS,[32] whereas **5** and **6** are much more selective in inhibiting hGGPPS. Triazole *E*/*Z*-**6** is currently the most potent hGGPPS inhibitor known (IC_{50} value of 45 nM).[35,36] Interestingly, the *E*/*Z* mixture of **6** is more potent than either one of its pure isomers and presumed to bind cooperatively in both the FPP substrate and the GGPP product subpockets of hGGPPS.[36] However, crystallographic confirmation of the exact binding mode of this compound has yet to be realized.

In this report, we present a novel chemotype of thienopyrimide-based bisphosphonate (ThP-BP; Figure 2) inhibitors of hGGPPS. Analogs **10a−d** and **11a−c** were identified that exhibit toxicity in various cancer cell lines and are particularly toxic to human myeloma cells, blocking prenylation and inducing apoptosis. The antimyeloma potency of some ThP-BP analogs is equivalent to that of doxorubicin while exhibiting far lower toxicity to healthy cells. Strong evidence of intracellular engagement of hGGPPS (by these inhibitors) was observed that correlates with their antimyeloma activity both in cellular assays and in vivo. The antimyeloma effects of prenylation inhibitors is a topic of significant interest. However, the necessity to develop selective inhibitors of hGGPPS has been intensely debated.[33] In principle, inhibitors of hFPPS are expected to directly block activation of FPP-dependent and indirectly GGPP-dependent GTPases; the latter as a consequence of intracellular depletion of the FPP substrate of hGGPPS (e.g., zoledronic acid blocks geranylgeranylation of Rap 1A[37]). In this report, we provide data from a large panel of human MM cell lines and MM patient bone marrow specimens suggesting that hGGPPS is a far more valuable therapeutic target for multiple myeloma than hFPPS.

RESULTS AND DISCUSION

Identification of hGGPPS Inhibitors and Confirmation of Binding to the Active Site. Libraries of structurally diverse thienopyrimidine-based bisphosphonates (ThP-BPs), substituted at the C-2, C-5, and/or the C-6 carbon of the parent molecule **7** (Figure 2), were synthesized in order to probe the molecular recognition elements differentiating between binding to hFPPS versus hGGPPS.[25,38,40] Approximately 200 analogs were screened in our in vitro assays for their ability to inhibit hFPPS and/or hGGPPS. In general, compounds substituted at C-5 (∼20 analogs) were found to be poor inhibitors of both enzymes; analogs more potent in inhibiting hFPPS were usually substituted at C-6 (∼100 analogs), whereas analogs substituted at C-2 (∼60 analogs) were inhibitors of hGGPPS with IC_{50} potency in the nanomolar range and exhibited selectivity against hFPPS. The synthesis of compounds having a C-2 substituent is briefly described in Scheme 1. The synthesis of this library was achieved using slightly modified literature procedures, as described in the Experimental Section; select examples are shown in Figure 2.

Initial structure−activity relationship (SAR) studies suggested that small substituents at either the C-2 or the C-6 position resulted in inhibitors with equivalent potency for both enzymes.[25,38] For example, the phenyl derivatives **8** and **9** (Figure 2) exhibited the same potency in inhibiting hGGPPS, with a narrow window of selectivity for hFPPS (Table 1). On the basis of these data, we initially presumed that rotation around the C-4 amino linker, connecting the thienopyrimidine scaffold to the bisphosphonate moiety, could allow the side chains of **8** and **9** to adopt similar enzyme-bound conformations. However, SAR optimization proved that higher selectivity for hGGPPS could be achieved by extending the side chain attached to the C-2 position. Inhibitor **10a** was found to exhibit in vitro potency (IC_{50}) of 64 nM in inhibiting hGGPPS and a selectivity window of approximately 30-fold against hFPPS (Table 1). In contrast, when the C-2 side chain of **10a** was transferred to the C-6 position of the thienopyrimidine core **7**, the resulting analog **12** was completely inactive in both in vitro inhibition assays at the highest concentration tested of 10 μM. These results confirmed that the molecular recognition elements involved in binding to hGGPPS (vs hFPPS) are not *simply* dictated by the presence of a bisphosphonate pharmacophore or the size and length of the side chain or the binding orientation of the thienopyrimidine scaffold. Further optimization of this class of compounds led to the identification of several hGGPPS inhibitors with IC_{50} values below 100 nM and a selectivity window of ≥15-fold. It is noteworthy that biological profiling of a 200-member library of ThP-BP compounds (a collection from this work and our previous studies[25,38,40]) clearly demonstrated that high potency in inhibiting hGGPPS, rather than hFPPS, is the critical factor in achieving nanomolar antitumor activity in human MM cells. Representative

Table 1. Enzyme Inhibition (IC_{50}) and Antiproliferation Activity (EC_{50}) in MM RPMI-8226 Cells of Representative ThP-BP Analogs[a]

	IC_{50} (μM)			EC_{50} (μM)
compd	hFPPS[b]	hGGPPS[b]	hGGPPS Y246D	RPMI-8226[c]
2	0.004	>100,000	nd	11
5	nd	0.43[d]	0.59	nd
7	∼0.8[e]	>1.0[e]	nd	nd
8	0.55	0.082	nd	nd
9	0.20	0.094	nd	nd
10a	2.0	0.064	0.039	0.50
10b	2.6	0.10	0.037	0.72
10c	1.0	0.085	0.092	nd
10d	>1.0[f]	0.042	nd	0.70
11a	3.0	0.049	0.050	0.46
11b	1.3	0.075	nd	0.23
11c	1.4	0.086	0.075	0.14[g]
12	IN	IN	nd	IN
13	0.023	1.5	nd	>100

[a]IN: inactive at the highest concentration tested of 10 μM. nd: not determined [b]IC_{50} values were determined with 10 min preincubation of the enzyme with each inhibitor; the values shown are average of $n \geq 3$ determinations with standard deviation of ±5−10%. [c]EC_{50} values were determined using an MTT assay after 72 h of incubation of the cells with or without an inhibitor; the values shown are average of $n \geq 4$ determinations with standard deviation of ≤2-fold. [d]IC_{50} value obtained in our own in vitro inhibition assays, when compounds were tested in parallel with several other analogs in above table. [e]Estimated values based on 70% and 40% inhibition observed for hFPPS and hGGPPS, respectively, at 1 μM. [f]20% inhibition was observed at 1 μM. [g]Average of five independent determinations, each run in quadruplicate.

DOI: 10.1021/acs.jmedchem.8b00886
J. Med. Chem. 2018, 61, 6904−6917

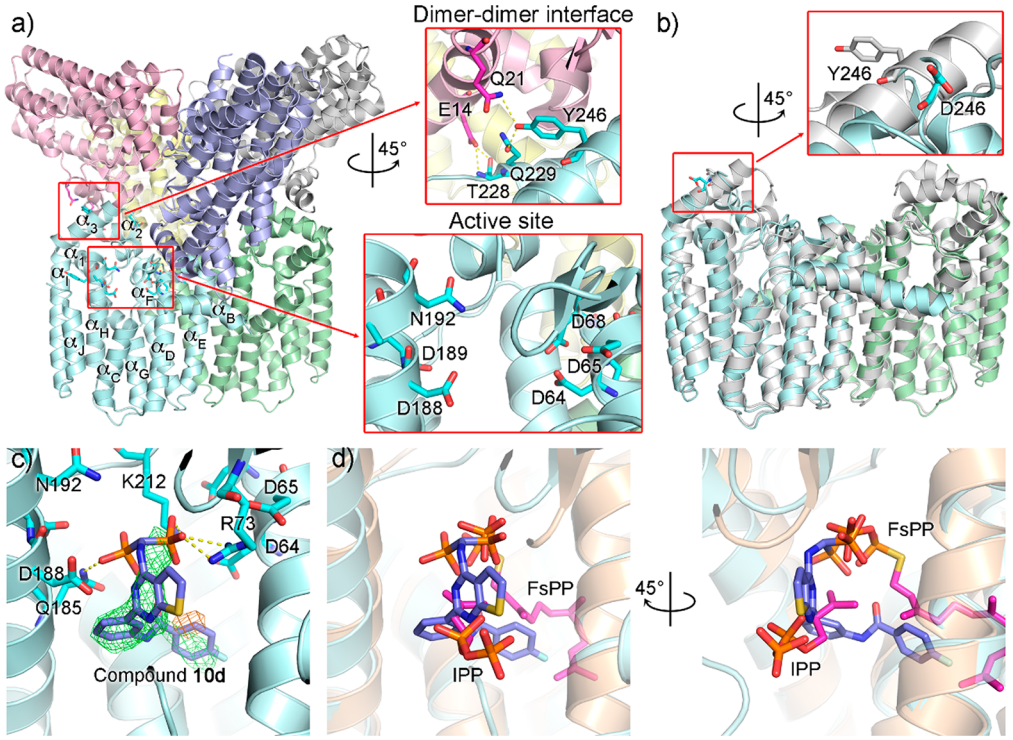

Figure 3. Crystal structure of wild type and mutant hGGPS. (a) Hexameric wild type hGGPPS (PDB entry 2Q80). Monomer units are indicated by different colors. (b) Dimeric hGGPPS mutant (Y246D; cyan and green; PDB entry 6C56). A dimer of the wild type enzyme (gray) is superposed (the inset highlights the single amino acid mutation disrupting the dimer−dimer contact). (c) Dimeric hGGPPS in complex with **10d** (PDB entry 6C57). The green and orange meshes represent the ligand discovery map (F_o - F_c contoured at 3σ) and the anomalous signal map (3σ), respectively. (d) Superposition of **10d**. GGPPS substrate with the structure of a sulfur derivative of FPP (FsPP) and IPP bound to the yeast enzyme (ligands in magenta; protein in semitransparent wheat; PDB entry 2E8T) are superimposed.

examples of ThP-BP hGGPPS inhibitors include analogs **10a−d** and the reversed amides **11a−c** (Figure 2).

Binding of the ThP-BP inhibitors to the active site of hGGPPS was confirmed by crystallography and DSF studies. Crystallization of the wild-type human GGPPS has proven to be very challenging, with only one structure reported so far.[39] We assumed that the multimeric organization of this enzyme, forming a trimer of homodimers (Figure 3a), may be responsible for this challenge. A more readily crystallizable Y246D mutant was created, disrupting the interdimer contacts mediated by Tyr 246 (Figure 3a).[39] This mutant is dimeric; it retains the same overall structure as the wild type enzyme (Figure 3b; PDB code 6C56; 2.80 Å resolution) and is catalytically competent (Table 1). We solved the cocrystal structure of inhibitor **10d** bound to the Y246D mutant, and despite lower resolution (PDB code 6C57; 3.50 Å resolution), we could observe the electron density for the inhibitor, as well as the anomalous signal from its sulfur atom, bound in the active site of one subunit (Figure 3c). While the exact binding conformation is unclear, the bisphosphonate of **10d** appears to bind between the aspartate-rich motifs, competing with the pyrophosphate of FPP (Figure 3d). Additionally, the *p*-fluorophenyl tail of **10d** appears to insert into the hydrophobic cavity formed between α_D and α_F, which typically accommodates the isoprenyl tail of FPP in the catalytic cycle. Binding of **10d** may also interfere with IPP binding, as the inhibitor's thienopyrimidine core extends into the second substrate site (Figure 3d). Binding of **10d** did not appear to involve Mg^{2+} ions (likely due to the low resolution), and it is plausible that direct interactions with residues Arg73, Gln185, and Lys212 can contribute to the stabilization of the charged bisphosphonate (Figure 3c). However, DSF studies clearly indicated that Mg^{2+} ions are required for the formation of the Y246D mutant/**10d** complex and an increase in thermal stability of the protein/inhibitor complex (Figure S3). Thus, our DSF data further corroborate that inhibitor **10d** binds to the active site of hGGPPS and must compete for binding with FPP.

Inhibition of Cancer Cell Proliferation and Rap1A Prenylation. Inhibitors of hGGPPS are known to block the proliferation of MM RPMI-8226 cells (e.g., *E*/*Z*-**6** was reported to exhibit an EC_{50} of 190 ± 58 nM).[35] Initial profiling of our ThP-BP library was carried out only for analogs exhibiting $IC_{50} \leq 100$ nM in inhibiting hGGPPS and a minimum of a 10-fold selectivity against hFPPS. Compounds were tested up to a maximum concentration of 10 μM; higher concentrations can lead to aggregation and artifacts.[40] Several compounds were identified exhibiting submicromolar potency in inhibiting the proliferation of RPMI-8226 cells with inhibitors **11b** and **11c** identified as the most potent analogs (Table 1; Figure 4a). As was expected, no inhibition was observed with the structurally related, inactive compound **12** or with ThP-BP inhibitors that preferentially target hFPPS, such as analog **13**, despite similar lipophilicity (as estimated by their relative retention on a C_{18} reversed phase HPLC column). These results strongly suggest that neither the bisphosphonate moiety nor inhibition of hFPPS are responsible for the antiproliferation activity observed with our hGGPPS inhibitors.

The hGGPPS inhibitor **11c** was approximately equally toxic to RPMI-8226 cells as doxorubicin (Figure 4a) and ∼80-fold more potent than zoledronic acid ($EC_{50} \sim 11$ μM). However,

DOI: 10.1021/acs.jmedchem.8b00886
J. Med. Chem. 2018, 61, 6904−6917

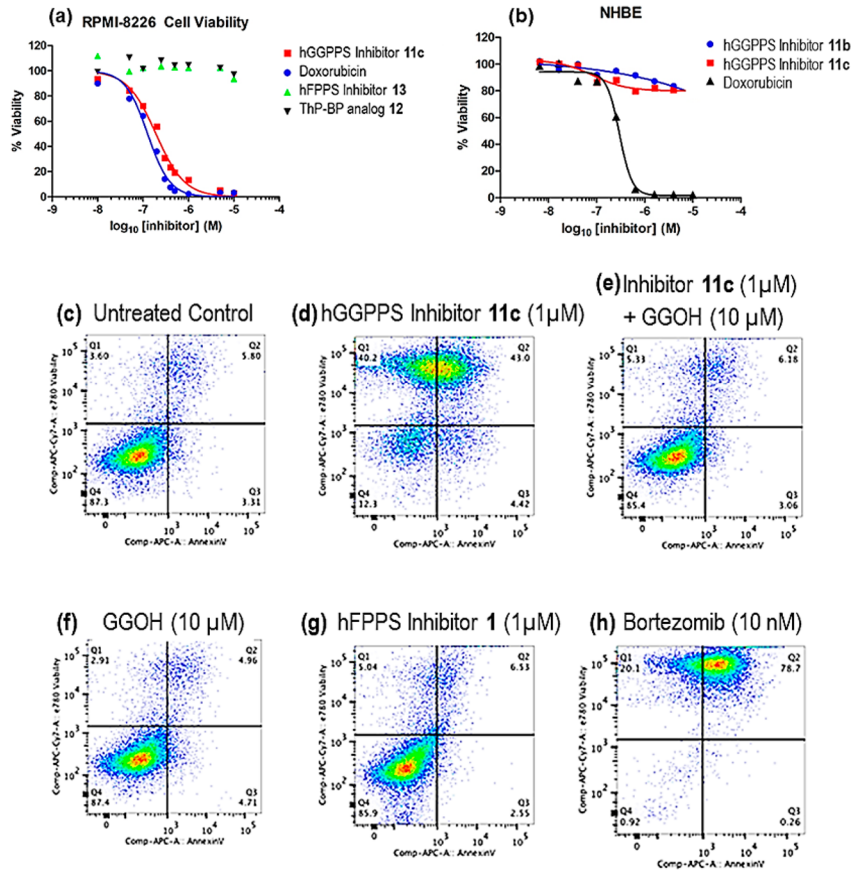

Figure 4. Antimyeloma properties of thienopyrimidine-based hGGPPS inhibitors. (a) Comparison of hGGPPS inhibitor **11c**, selective hFPPS inhibitor **13**, and inactive ThP-BP compound **12**. Doxorubicin was used as a positive control. (b) Toxicity effects on normal human bronchial cells (NHBE) induced by inhibitors **11b**, **11c**, and doxorubicin. Apoptosis of MM RPMI-8226 cells after 72 h of incubation with (c) vehicle, (d) inhibitor **11c**, (e) GGOH and inhibitor **11c**, (f) GGOH alone, (g) ZOL (**1**) at the same concentration as **11c**, and (h) bortezomib.

11c was significantly less toxic to normal bronchial cells (NHBE) than doxorubicin, which exhibited an EC_{50} of ~300 nM (Figure 4b). Antimyeloma potency (EC_{50} ~ 100−500 nM) was also observed in a genetically diverse panel of MM cell lines characteristic of the human disease, including cells carrying NF-κB activation mutations, RAS mutations, and p53 mutations/deletions (e.g., Figure S4a).[41] Given that cancers harboring genetic anomalies in p53 are commonly resistant to standard chemotherapy,[42] the latter is an important observation. The antitumor effects of inhibitors **11b** and **11c** were also evaluated in a variety of other cancer cell lines with K-Ras/N-Ras overexpression and/or activating mutations, as well as an ovarian cancer cell line expressing high levels of multidrug resistant pumps (e.g., ADR-RES), along with doxorubicin as a control. In spite of their lower toxicity in normal cells, inhibitors **11b**/**11c** appeared to be as effective as (*or better than*) doxorubicin in blocking the proliferation of ADR-RES cells (Figure S4b). Antitumor activity was also observed in pancreatic cancer (MiaPaCa-2) and other cancer cells with several ThP-BP analogs (examples shown in Figure S4c). Interestingly, the toxicity of analog **11b** in MiaPaCa-2 cells was stronger than that of L-778,123 (**3**), in spite of its bisphosphonate chemical nature. L-778,123 was advanced to phase I clinical trials in patients with pancreatic cancer (90% K-Ras mutations, but was withdrawn from development due to toxicity.[29]

Intracellular Engagement of hGGPPS, Induction of Cell Apoptosis, and Inhibition of Rap 1A Prenylation. Evaluation of several ThP-BP analogs by flow cytometry confirmed that they induce apoptosis in RPMI-8226 cells in a dose-depended manner; zoledronic acid (**1**) and the antimyeloma drug bortezomib (a proteosome inhibitor) were used as controls. Apoptosis of RPMI-8226 cells was observed with many hGGPPS inhibitors, including compounds **10b** (Figure S5) and **11c** (Figure 4d). In contrast, no apoptosis was observed with **1**, when tested in parallel at the same concentration (Figure 4g). Although induction of apoptosis in cancer cells treated with *N*-BP inhibitors of hFPPS has been previously reported (e.g., with incadronate in MM[43] and breast cancer[44] and with **1** in renal carcinoma[45] and mesothelioma[46] cells), these observations were possible only at very high concentrations of compound. Interestingly, in many of these studies greater reduction of toxicity was observed when cells were co-treated with geranylgeraniol (GGOH) than with farnesol (FOH).[47] However, such observations cannot be interpreted as proof that intracellular depletion of GGPP is more toxic to cancer cells than depletion of FPP, since neither the relative cell permeability of FOH and GGOH nor their relative rates of bioconversion to their corresponding pyrophosphate metabolites are known. In our studies, complete rescue from apoptosis was observed when cells were simultaneously treated with a toxic dose of inhibitor **11c** and a nontoxic dose of geranylgeraniol (GGOH; Figure 4e and Figure 4f, respectively). These results are consistent with selective intracellular target engagement and a mechanism-based toxicity due to inhibition of hGGPPS. However, since

DOI: 10.1021/acs.jmedchem.8b00886
J. Med. Chem. 2018, 61, 6904−6917

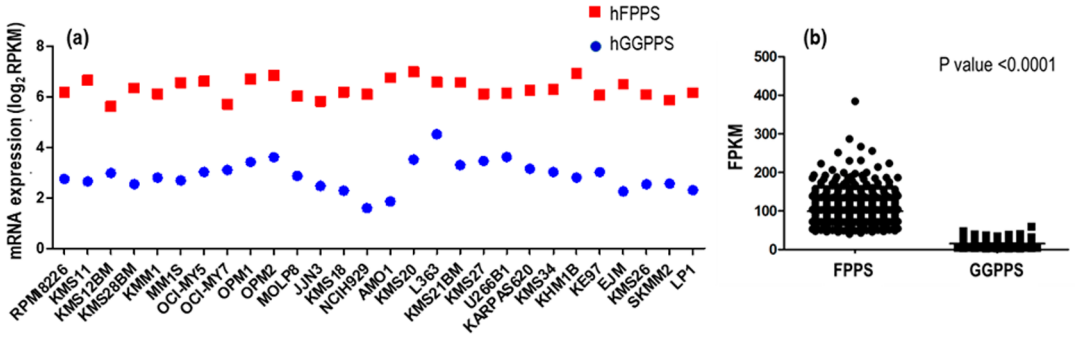

Figure 5. RNA transcript level (RNAseq) of hFPPS and hGGPPS. (a) mRNA expression (Log_2 RPKM) of hFPPS and hGGPPS in various human MM cell lines. (b) mRNA expression levels (FPKM) of hFPPS and hGGPPS in CD138-selected MM cells from patients' bone marrow specimens obtained at diagnosis.

bisphosphonates act as bioisosteres of isoprenoid metabolites, it is conceivable that in addition to inhibiting hGGPPS, our ThP-BP compounds could also potentially inhibit the transferase enzymes (e.g., GGTase I and II), an effect that may be possible to overcome by high concentrations of GGOH. More in-depth studies are required to completely rule out any additional off-target effects. We also used bortezomib to induce apoptosis (Figure 4h) and observed no rescue when cells were co-treated with this drug and GGOH (Figure S5), consistent with a mechanism of action that is independent of protein prenylation.

The ability of our hGGPPS inhibitors to disrupt intracellular geranylgeranylation of small GTPases was confirmed. For example, RPMI-8226 cells were incubated with increasing concentrations of inhibitor **11c** and their lysate was analyzed by Western Blotting, using a Rap 1A antibody that specifically binds to the unprenylated form of the protein. Dose-dependent inhibition of Rap 1A prenylation was observed at concentrations as low as 150−200 nM; similar results were observed with zoledronic acid (**1**) at approximately 0.5 μM concentration (Figure S6).

Impairment of isoprenoid biosynthesis has been previously reported to also disrupt secretory pathway function in MM cells, leading to the accumulation of intracellular immunoglobulins and/or light chains in the endoplasmic reticulum (ER) that leads to ER stress-induced apoptosis.[48] We confirmed similar results with inhibitor **11c**, which induced increased splicing of XBP1 mRNA, as a consequence of ER stress (Figure S7a). Moreover, the increased XBP1 mRNA splicing caused by **11c** was largely subverted by simultaneous co-treatment with GGOH, consistent with ER stress induction due to hGGPPS inhibition. Western blot analysis also demonstrated that XBP1s (the protein product of spliced XBP1 mRNA) increased with hGGPPS inhibitor treatment, and this effect was also mitigated by GGOH co-treatment (Figure S7b). Increased and decreased phosphorylation of ERK and AKT, respectively, was also observed (Figure S7b). Collectively, these results suggest that intracellular inhibition of hGGPPS produces proapoptotic ERK signaling and concomitant loss of prosurvival AKT signaling in MM cells.

From a biochemical perspective, a reasonable first assumption is that the inhibition of hFPPS should block all downstream events in the mevalonate pathway, thus blocking prenylation of GTPases and inducing cell apoptosis. However, our results suggest that hGGPPS plays a more important role in cancer cell biology than hFPPS. Although the low cell-based potency of zoledronic acid (**1**) may be attributed to its poor physicochemical properties, we observed a dramatic difference in antimyeloma efficacy with structurally very similar ThP-BP compounds that preferentially inhibit hGGPPS vs hFPPS (e.g., hFPPS inhibitor **13** vs hGGPPS inhibitor **11c**; Figure 4a), suggesting that hGGPPS may be a better therapeutic target for oncology. To gain some insight into the reasons for our observations, we analyzed the intracellular level of these biological targets that potentially need to be engaged by an inhibitor, as can be inferred from the abundance of mRNA transcripts of each enzyme in cells.[49] We found that the mRNA levels of hFPPS are consistently higher than those of hGGPPS in all human MM cells (Figure 5a). Similar differences in the mRNA levels were observed in primary cancer cells, taken from bone marrow specimens (obtained at diagnosis) of over 700 MM patients participating in a large clinical trial (Figure 5b; CoMMpass IA10 clinical trial data (NCT01454297)].[50−52] Collectively, the mRNA data strongly suggest that a lower dose of a drug would be required to achieve a much higher level of intracellular engagement of hGGPPS (thus potentially leading to better clinical efficacy and greater therapeutic index) than with an inhibitor of hFPPS. This conclusion is based on the assumption that the two inhibitors (for hGGPPS vs hFPPS) have equivalent potency and similar overall biopharmaceutical profiles.

Preclinical Evaluation of a ThP-BP Inhibitor: Metabolic Stability, Bone Affinity, and Proof-of-Principle Studies. The half-life clearance of inhibitor **11c** in male CD-1 mouse (MLM), Sprague-Dawley rat (RLM), and human (HLM) liver microsomes was found to be 128 min, 187 min, and 154 min, respectively. Given the strong association between the MM malignancy and lytic bone disease, as well as the relationship between protein geranylgeranylation and bone resorbing osteoclasts,[53] the affinity of our ThP-BP compounds for the bone mineral hydroxyapatite (HAP) was of significant importance. A validated ^{1}H NMR protocol was used to estimate the affinity of our compounds for bone.[54] The relative affinity of analogs **11a** and **11c** for hydroxyapatite (HAP) was found to be equivalent to that of zoledronic acid and slightly stronger than that of risedronic acid (^{1}H NMR data in Figure S8).

Encouraged by the above data, the in vivo efficacy of inhibitor **11c** was subsequently investigated in a validated MM mouse model that recapitulates the characteristics of the human MM disease and mimics the therapeutic responses of MM patients to clinically validate drugs.[55] Vk*MYC transgenic mice were bred and maintained in a pathogen-free standard animal facility with a light/dark cycle of 12 h and provided

DOI: 10.1021/acs.jmedchem.8b00886
J. Med. Chem. 2018, 61, 6904−6917

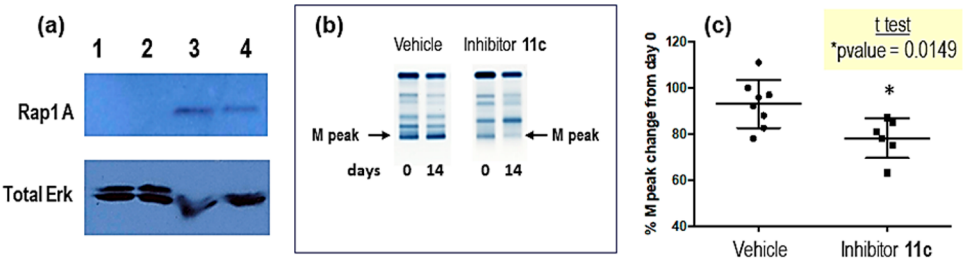

Figure 6. (a) Western blot analysis of two representative PBMC samples from vehicle (lanes 1 and 2) and inhibitor **11c** treated mice (lanes 3 and 4). (b) Serum protein electrophoresis from animals treated with vehicle or inhibitor **11c**. Arrows indicated location of M-protein. (c) Analysis of M-protein as a percentage of total serum protein and expressed as a change from baseline (day 0) to day 14 for each respective mouse. Statistical analysis was performed using unpaired two-tailed Student's *t* test.

with food and water ad libitum. They were observed daily for any signs of overt toxicity, such as significant weight loss, decreased mobility, skin lesions, inflammation at the site of injection, or morbidity, according to the Facility Animal Care Committees Protocol Number 2012-7242 from the Research Institute of McGill University Health Center (RI MUHC; Glen site) and in accordance with the Policies and Guidelines of the Canadian Council on Animal Care (CCAC).

Aged mice (average 50 weeks old)[56] with disease measurable by serum protein electrophoresis (i.e., M-protein levels higher than 15% of total serum proteins, a biomarker of MM disease burden) were treated with 3 mg kg^{-1} day^{-1} of compound **11c** or vehicle (phosphate buffered saline; PBS) by intraperitoneal injection (ip; $n = 8$ per group, age and gender matched) over a period of 14 days (a total of 12 doses, with a drug holiday during the weekends). Weight loss was observed in all animals over the treatment period, ranging from ~10% ($n = 4$) to 16% ($n = 2$) in the control group and 15% ($n = 4$) to 28% ($n = 1$) for the animals treated with **11c** (two of the animals in the latter group were euthanized on day 13). Some of the weight loss was attributed to stress induced by daily intraperitoneal injections and manipulation of the animals. At the end of treatment with **11c**, Western blot analysis of peripheral blood mononuclear cell (PBMC) lysates clearly showed inhibition of Rap 1A geranylgeranylation, which is the expected and desired outcome of hGGPPS inhibition, providing evidence of systemic exposure and in vivo target engagement (Figure 6a). Encouraging antimyeloma efficacy was also observed with a decrease in serum M-protein for the mice treated with **11c** as compared to an increase for animals treated with vehicle (Figure 6b,c). Since the half-life of mouse immunoglobulins (i.e., M-protein) is approximately 7 days,[57] the observed decrease in M-protein after less than 2 weeks of treatment (*albeit moderate*) is an exciting result that clearly proves the in vivo antimyeloma efficacy of inhibitor **11c**. It is noteworthy that for this study, daily dosing of compound **11c** (or vehicle) was carried out by ip injection, since daily dosing of mice by iv is impractical and requires implanted slow delivery iv pumps. A disadvantage to ip administration of drugs is lower systemic exposure (as compared to iv dosing) and increased absorption into the liver (due to direct transport from the peritoneal cavity into the portal vein system); the latter leads to higher potential for hepatic toxicity. Blood chemistry assessment of plasma samples (collected at the end of the study) confirmed increased alanine transaminase (ALT) and aspartate transaminase (AST) levels in some animals treated with **11c**, although the levels were highly variable (see Table S3). However, there was no correlation between the increase of liver enzymes, extent of weight loss, and decrease of M-protein levels for the animals treated with **11c** that could potentially imply a mechanism-based toxicity.

CONCLUSION

Multiple myeloma (MM) is a malignancy of B lymphocytes, characterized by the accumulation of malignant plasma cells in the bone marrow that secrete monoclonal immunoglobulins (M-protein) and give rise to a constellation of target organ damage known as CRAB (hypercalcemia, renal failure, anemia, bone disease).[58] In the past, inhibition of protein prenylation of small GTPases that are intimately involved in oncogenesis was proposed as a plausible mechanism of MM therapy. However, strong clinical proof of efficacy with inhibitors of hFPPS, FTase, and GGTase I inhibitors has been elusive. Currently, there are no known clinically validated inhibitors of hGGPPS. A new chemotype of hGGPPS inhibitors, represented by compound **11c**, was identified and found to induce antimyeloma effects both in vitro and in a reliable MM disease mouse model, which has been shown to accurately predict human drug response.

The studies herein also provide substantial evidence that the hGGPPS is a better therapeutic target for the treatment of MM than the upstream enzyme of the isoprenoid biosynthetic cascade (hFPPS). Support for this hypothesis was provided by antiproliferation data in human MM cells, which clearly showed a stronger response to compounds inhibiting hGGPPS, as compared to structurally related analogs (i.e., having very similar physicochemical properties) that are more potent at inhibiting hFPPS. Additionally, analysis of the mRNA levels of hFPPS and hGGPPS in MM cancer cells and bone marrow specimens of MM patients indicated much higher intracellular mRNA levels of hFPPS than hGGPPS. Collectively, these observations suggest that assuming selective hFPPS and hGGPPS inhibitors were identified that possessed equivalent biopharmaceutical properties, a more effective target engagement and better clinical outcome would be expected with therapeutic agents targeting hGGPPS. Furthermore, it has been proposed that the beneficial effects of *N*-BPs on bone resorption are more likely the result of indirect inhibition of geranylgeranylation (rather than direct farnesylation) of proteins in osteoclasts.[59] As one of the salient features of human MM is osteolytic bone disease, compounds such as **11c** that bind to bone with high affinity (thereby concentrating in the milieu of the MM disease), inhibit geranylgeranylation (thus blocking bone resorption), and exhibit strong antimyeloma activity may provide the ideal set of therapeutic properties for the treatment of multiple myeloma.

DOI: 10.1021/acs.jmedchem.8b00886
J. Med. Chem. 2018, 61, 6904−6917

EXPERIMENTAL SECTION

General Chemistry. Chemicals and solvents were purchased from commercial suppliers and used without further purification. Normal phase column chromatography on silica gel was performed using a CombiFlash instrument using the solvent gradient, as indicated. Reverse phase preparative HPLC was carried out using a Waters Atlantis Prep T3 OBD C18 5 μm, 19 mm × 50 mm column. Solvent A: H_2O, 0.1% formic acid. Solvent B: CH_3CN, 0.1% formic acid. Mobile phase: gradient from 95% A and 5% B to 5% A and 95% B in 17 min acquisition time. Flow rate: 1 mL/min. The homogeneity of final inhibitors was confirmed to be ≥95% by reversed-phase HPLC using a Waters ALLIANCE instrument (e2695 with 2489 UV detector, 3100 mass spectrometer, C18 5 μm column). Solvent A: H_2O, 0.1% formic acid. Solvent B: CH_3CN, 0.1% formic acid. Mobile phase: linear gradient from 95% A and 5% B to 0% A and 100% B in 13 min. Key compounds were fully characterized by ^1H, ^{13}C, ^{31}P NMR and HRMS. Chemical shifts (δ) are reported in ppm relative to the internal deuterated solvent. The NMR spectra of all final bisphosphonate inhibitors were acquired in D_2O (either after conversion to their corresponding trisodium salt or by addition of ~2% ND_4OD) or in DMSO-d_6. In some cases, the Cα to the bisphosphonate was broad and overlapped with the solvent peak, as confirmed by HSQC NMR studies. The high resolution MS spectra of final products were recorded using electrospray ionization ($ESI^{\pm}$) and Fourier transform ion cyclotron resonance mass analyzer (FTMS). The HRMS data for inhibitors **10a−c**, **11a−c**, and **12** were acquired from the corresponding trisodium salt of the bisphosphonic acid.

General Protocols for the Synthesis of Inhibitors 10 and 11. Amide Bond Formation. Method A. To a stirring solution of intermediate **18** (80 mg, 0.15 mmol) in dry DCM (1.5 mL) at 0 °C, dry Et_3N (97 μL, 0.45 mmol) was added, followed by an acid chloride (aryl-COCl or heteroary-COCl; 0.18 mmol), which was added dropwise. The solution was stirred and allowed to warm to rt (reaction progress was monitored by TLC or LC−MS). Once complete (typically, after ~1 h), the reaction was poured into sat. $NaHCO_3$ solution and extracted with EtOAc (2×), washed with brine, dried over anhydrous Na_2SO_4, and concentrated under vacuum. Crude product was purified by silica gel column chromatography using a gradient from 25% EtOAc in hexanes to 100% EtOAc and then to 20% MeOH in EtOAc. Product typically eluted with 10−20% MeOH in EtOAc. Isolated yields typically ranged from 75% to quantitative.

Amide Bond Formation. Method B. Alternatively, to a mixture of intermediate **19** (50 mg, 0.09 mmol) and an amine (aryl-NH_2 or heteroaryl-NH_2) (0.1 mmol) in dry DMF (2.0 mL), DIPEA (31 μL, 0.18 mmol) was added, followed by HBTU (37.4 mg, 0.1 mmol). The solution was stirred at rt until complete conversion was observed by TLC (typically after ~1−2 h). The reaction mixture was then diluted with brine and was extracted with EtOAc. The organic phase was washed with sat. NH_4Cl solution, brine, dried over anhydrous Na_2SO_4, and concentrated in vacuo. Crude product was purified by silica-gel column chromatography as described for method A above. Isolated yields typically ranged from 60% to 80%.

Step 2. General Protocol for Conversion of the Bisphosphonate Esters to the Bisphosphonic Acids. Deprotection was carried out using TMSBr, followed by methanolysis previously described.[38] Isolated yields ranged from 40% to 90%.

(((2-(3-Benzamidophenyl)thieno[2,3-*d*]pyrimidin-4-yl)amino)methylene)bis(phosphonic acid) (10a). The tetraethyl (((2-(3-benzamidophenyl)thieno[2,3-*d*]pyrimidin-4-yl)amino)methylene)bis(phosphonate) was isolated as a light yellow solid. ^1H NMR (500 MHz, DMSO-d_6): δ 10.43 (s, -NH), 8.86 (t, J = 1.7 Hz, 1H), 8.65 (d, J = 9.7 Hz, -NH), 8.12 (d, J = 7.9 Hz, 1H), 8.10 (d, J = 6.0 Hz, 1H), 8.01 (d, J = 7.1 Hz, 2H), 7.91 (dd, J = 8.1, 1.1 Hz, 1H), 7.64 (d, J = 6.0 Hz, 1H), 7.63−7.59 (m, 1H), 7.57−7.53 (m, 2H), 7.51 (t, J = 7.9 Hz, 1H), 6.06 (td, J = 23.3, 9.5 Hz, 1H), 4.18−4.07 (m, 8H), 1.19−1.10 (m, 12H). ^{31}P NMR (203 MHz, DMSO-d_6) δ 17.01 (s).

Inhibitor **10a** was isolated as a pale yellow solid. ^1H NMR (400 MHz, D_2O): δ 8.36 (s, 1H), 8.18 (d, J = 7.9 Hz, 1H), 7.95 (d, J = 7.3 Hz, 2H), 7.89 (d, J = 8.2 Hz, 1H), 7.70−7.57 (m, 5H), 7.49 (d, J = 6.0 Hz, 1H), 5.13 (t, J = 18.6 Hz, 1H). ^{31}P NMR (162 MHz, D_2O): δ 13.79 (s). ^{13}C NMR (101 MHz, D_2O): δ 169.8, 165.5, 159.8, 157.0, 138.7, 137.5, 133.9, 132.4, 129.5, 128.8, 127.4, 125.3, 124.3, 123.1, 122.0, 119.0, 115.9. C-α to the bisphosphonate was observed by HSQC. HSQC ($^1H-^{13}C$): ^1H at δ 5.13 correlates to ^{13}C-α at δ 49.5. HRMS [ESI^+] calculated for $C_{20}H_{16}N_4Na_3O_7P_2S$ m/z, 586.9903; found 586.9898 $[M + H]^+$.

(((2-(3-(4-Methylbenzamido)phenyl)thieno[2,3-*d*]pyrimidin-4-yl)amino)methylene)bis(phosphonic acid) (10b). The tetraethyl (((2-(3-(4-methylbenzamido)phenyl)thieno[2,3-*d*]pyrimidin-4-yl)amino)methylene)bis(phosphonate) was isolated as a pale yellow solid. ^1H NMR (500 MHz, DMSO-d_6): δ 10.34 (s, -NH), 8.85 (t, J = 1.8 Hz, 1H), 8.65 (d, J = 9.7 Hz, -NH), 8.12−8.09 (m, 2H), 7.93 (d, J = 8.2 Hz, 2H), 7.91 (ddd, J = 8.1, 2.1, 1.0 Hz, 1H), 7.64 (d, J = 6.0 Hz, 1H), 7.50 (t, J = 7.9 Hz, 1H), 7.35 (d, J = 7.9 Hz, 2H), 6.06 (td, J = 23.4, 9.7 Hz, 1H), 4.18−4.05 (m, 8H), 2.40 (s, 3H), 1.19−1.10 (m, 12H). ^{31}P NMR (203 MHz, DMSO-d_6): δ 17.00 (s). MS [ESI^+] m/z: 647.2 $[M + H^+]^+$.

Inhibitor **10b** was isolated as a pale yellow solid. ^1H NMR (500 MHz, D_2O): δ 8.38 (s, 1H), 8.20 (d, J = 7.6 Hz, 1H), 7.93 (d, J = 7.1 Hz, 1H), 7.89 (d, J = 7.9 Hz, 2H), 7.68−7.63 (m, 2H), 7.51 (d, J = 5.9 Hz, 1H), 7.46 (d, J = 7.9 Hz, 2H), 5.15 (t, J = 18.9 Hz, 1H), 2.47 (s, 3H). ^{31}P NMR (203 MHz, D_2O) δ 13.82 (s). ^{13}C NMR (101 MHz, D_2O): δ 169.3, 165.6, 159.5, 156.8, 143.5, 138.3, 137.5, 130.7, 129.4, 129.3, 127.5, 125.0, 124.1, 123.3, 121.6, 118.8, 115.8, 48.9 (t, J = 124.8 Hz), 20.6. HRMS [ESI^+] calculated for $C_{21}H_{18}N_4Na_3O_7P_2S$ m/z, 601.00590; found 601.00773 $[M + H]^+$.

(((2-(3-(4-Methoxybenzamido)phenyl)thieno[2,3-*d*]pyrimidin-4-yl)amino)methylene)bis(phosphonic acid) (10c). The tetraethyl (((2-(3-(4-methoxybenzamido)phenyl)thieno[2,3-*d*]pyrimidin-4-yl)amino)methylene)bis(phosphonate) was isolated as a pale yellow solid. ^1H NMR (500 MHz, DMSO-d_6): δ 10.27 (s, -NH), 8.84 (t, J = 1.7 Hz, 1H), 8.65 (d, J = 9.7 Hz, -NH), 8.11−8.09 (m, 2H), 8.02 (d, J = 8.8 Hz, 2H), 7.90 (dd, J = 6.9, 1.2 Hz, 1H), 7.64 (d, J = 6.0 Hz, 1H), 7.49 (t, J = 7.9 Hz, 1H), 7.08 (d, J = 8.9 Hz, 2H), 6.06 (td, J = 23.4, 9.7 Hz, 1H), 4.18−4.07 (m, 8H), 3.85 (s, 3H), 1.19−1.10 (m, 12H). ^{31}P NMR (203 MHz, DMSO-d_6): δ 17.01 (s). MS [ESI^+] m/z: 663.2 $[M + H^+]^+$.

Inhibitor **10c** was isolated as pale yellow solid. ^1H NMR (400 MHz, D_2O): δ 8.36 (s, 1H), 8.19 (d, J = 7.8 Hz, 1H), 7.98 (d, J = 8.8 Hz, 2H), 7.91 (d, J = 8.1 Hz, 1H), 7.68−7.60 (m, 2H), 7.50 (d, J = 6.0 Hz, 1H), 7.17 (d, J = 8.9 Hz, 2H), 5.11 (t, J = 19.0 Hz, 1H), 3.94 (s, 3H). ^{31}P NMR (162 MHz, D_2O) δ 13.78 (s). ^{13}C NMR (126 MHz, D_2O): δ 169.1, 165.0, 162.2, 160.0, 156.8, 138.7, 137.6, 129.6, 129.5, 126.3, 125.1, 124.4, 122.6, 122.0, 119.2, 116.0, 114.1, 55.5. C-α to the bisphosphonate was observed by HSQC. HSQC ($^1H-^{13}C$): ^1H at δ 5.11 correlates to ^{13}C-α at δ 50.0. HRMS [ESI^+] calculated for $C_{21}H_{18}N_4Na_3O_8P_2S$ m/z, 617.000 82; found 617.001 81 $[M + H]^+$

(((2-(3-(4-Fluorobenzamido)phenyl)thieno[2,3-*d*]pyrimidin-4-yl)amino)methylene)bis(phosphonic acid) (10d). The tetraethyl (((2-(3-(4-fluorobenzamido)phenyl)thieno[2,3-*d*]pyrimidin-4-yl)amino)methylene)bis(phosphonate) was isolated as a pale yellow solid (48 mg, 65%). ^1H NMR (500 MHz, $CDCl_3$): δ 8.39 (s, 1H), 8.28 (d, J = 7.9 Hz, 1H), 8.14 (d, J = 7.6 Hz, 1H), 8.03−7.90 (m, 3H), 7.52 (t, J = 8.0 Hz, 1H), 7.37 (d, J = 6.0 Hz, 1H), 7.21 (t, J = 8.5 Hz, 2H), 5.97 (d, J = 9.9 Hz, 1H), 5.78 (s, 1H), 4.35−4.08 (m, 8H), 1.29−1.19 (m, 12H). ^{31}P NMR (203 MHz, $CDCl_3$): δ 16.84.

Inhibitor **10d** was isolated as a light beige solid (26.1 mg, 63%). ^1H NMR (400 MHz, D_2O): δ 8.37 (s, 1H), 8.20 (d, J = 7.9 Hz, 1H), 8.05−7.98 (m, 2H), 7.93 (d, J = 8.1 Hz, 1H), 7.70−7.60 (m, 2H), 7.51 (d, J = 6.0 Hz, 1H), 7.39−7.29 (m, 2H), 5.17 (t, J = 19.0 Hz, 1H). ^{31}P NMR (162 MHz, D_2O): δ 13.93 (s). ^{13}C NMR (126 MHz, D_2O): δ 168.5, 165.8, 165.4, 163.8, 159.7, 156.9, 138.5, 137.4, 130.1, 130.0, 129.4, 125.1, 124.1, 122.9, 121.7, 118.9, 115.8, 115.7, 115.5, 49.5 (t, J = 122.7 Hz). HRMS [ESI^-] calculated for $C_{20}H_{15}FN_4NaO_7P_2S$ m/z $[M - 2H + Na]^-$ 559.0024; found 559.0010 $[M - 2H + Na]^-$.

(((2-(3-(Phenylcarbamoyl)phenyl)thieno[2,3-*d*]pyrimidin-4-yl)amino)methylene)bis(phosphonic acid) (11a). The tetraethyl

DOI: 10.1021/acs.jmedchem.8b00886
J. Med. Chem. 2018, 61, 6904−6917

(((2-(3-(phenylcarbamoyl)phenyl)thieno[2,3-*d*]pyrimidin-4-yl)-amino)methylene)bis(phosphonate) was isolated as a light yellow solid. ^{1}H NMR (400 MHz, DMSO-d_6): δ 10.47 (s, -NH), 8.95 (s, 1H), 8.75 (d, J = 9.6 Hz, -NH), 8.57 (d, J = 7.9 Hz, 1H), 8.10 (d, J = 5.7 Hz, 1H), 8.07 (d, J = 7.9 Hz, 1H), 7.82 (d, J = 7.7 Hz, 2H), 7.71−7.66 (m, 2H), 7.39−7.35 (m, 2H), 7.12 (t, J = 7.4 Hz, 1H), 6.03 (br, 1H), 4.18−4.00 (m, 8H), 1.19−1.08 (m, 12H). ^{31}P NMR (162 MHz, DMSO-d_6) δ 17.05 (s). ^{13}C NMR (126 MHz, DMSO-d_6): δ 167.6, 165.5, 157.5, 156.0 (t, J = 3.7 Hz), 139.2, 137.7, 135.5, 130.4, 129.4, 128.7, 128.6, 127.1, 123.8, 123.7, 120.3, 120.2, 115.5, 62.9−62.7 (m), 16.2−16.1 (m). C-α to the bisphosphonate was observed by HSQC. HSQC (^{1}H−^{13}C): ^{1}H at δ 6.03 correlates to ^{13}C-α at δ 45.1. MS [ESI$^+$] m/z: 633.2 [M + H$^+$]$^+$.

Inhibitor **11a** was isolated as off-white solid. ^{1}H NMR (400 MHz, D_2O): δ 8.81 (s, 1H), 8.58 (d, J = 7.9 Hz, 1H), 8.06 (d, J = 7.8 Hz, 1H), 7.76 (t, J = 7.8 Hz, 1H), 7.66−7.63 (m, 3H), 7.56−7.52 (m, 3H), 7.36 (t, J = 7.4 Hz, 1H), 5.20 (t, J = 19.0 Hz, 1H). ^{31}P NMR (203 MHz, D_2O): δ 13.91 (s). ^{13}C NMR (126 MHz, D_2O): δ 169.4, 165.5, 159.7, 157.0, 138.3, 136.9, 134.4, 132.0, 129.4, 129.3, 129.2, 126.9, 126.0, 123.2, 123.0, 119.0, 115.9, 49.3 (^{13}C-α observed by HSQC). HSQC (^{1}H−^{13}C): ^{1}H at δ 5.20 correlates to ^{13}C-α at δ 49.3. HRMS [ESI$^+$] calculated for $C_{20}H_{16}N_4Na_3O_7P_2S$ m/z, 586.9903; found 586.9903 [M + H]$^+$.

(((2-(3-((4-Methoxyphenyl)carbamoyl)phenyl)thieno[2,3-*d*]-pyrimidin-4-yl)amino)methylene)bis(phosphonic acid) (11b). The tetraethyl (((2-(3-((4-methoxyphenyl)carbamoyl)phenyl)thieno-[2,3-*d*]pyrimidin-4-yl)amino)methylene)bis(phosphonate) was isolated as a light yellow solid. ^{1}H NMR (500 MHz, $CDCl_3$ with ~0.1% CD_3OD): δ 9.01 (s, 1H), 8.67 (br_s, 1H), 8.59 (d, J = 7.8 Hz, 1H), 8.11 (d, J = 7.6 Hz, 1H), 7.68 (d, J = 8.8 Hz, 2H), 7.61 (t, J = 7.7 Hz, 1H), 7.45 (d, J = 5.3 Hz, 1H), 7.37 (d, J = 6.0 Hz, 1H), 6.92 (d, J = 9.0 Hz, 2H), 5.86 (t, J = 22.3 Hz, 1H), 4.27−4.10 (m, 8H), 3.82 (s, 3H), 1.26 (t, J = 7.1 Hz, 6H), 1.21 (t, J = 7.1 Hz, 6H). ^{31}P NMR (203 MHz, $CDCl_3$): δ 17.10 (s). MS [ESI$^+$] m/z: 663.4 [M + H$^+$]$^+$.

Inhibitor **11b** was isolated as off-white solid. ^{1}H NMR (500 MHz, D_2O): δ 8.74 (s, 1H), 8.54 (d, J = 7.8 Hz, 1H), 8.00 (d, J = 7.7 Hz, 1H), 7.72 (t, J = 7.8 Hz, 1H), 7.62 (d, J = 5.9 Hz, 1H), 7.51−7.49 (m, 3H), 7.06 (d, J = 8.9 Hz, 2H), 5.18 (t, J = 18.9 Hz, 1H), 3.86 (s, 3H). ^{13}C NMR (126 MHz, D_2O): δ 169.3, 165.5, 159.7, 157.0, 156.7, 138.3, 134.3, 132.0, 130.1, 129.3, 129.3, 126.8, 124.8, 123.2, 118.9, 115.9, 114.4, 55.5, 49.3 (^{13}C-α observed by HSQC). HSQC (^{1}H−^{13}C): ^{1}H at δ 5.18 correlates to ^{13}C-α at δ 49.3. ^{31}P NMR (203 MHz, D_2O): δ 13.91 (s). HRMS [ESI$^+$] calculated for $C_{21}H_{18}N_4Na_3O_8P_2S$ m/z, 617.000 82; found 617.000 90 [M + H$^+$]$^+$.

(((2-(3-((3-Fluoro-4-methoxyphenyl)carbamoyl)phenyl)-thieno[2,3-*d*]pyrimidin-4-yl)amino)methylene)bis-(phosphonic acid) (11c). The tetraethyl (((2-(3-((3-fluoro-4-methoxyphenyl)carbamoyl)phenyl)thieno[2,3-*d*]pyrimidin-4-yl)-amino)methylene)bis(phosphonate) was isolated as a yellow solid. ^{1}H NMR (500 MHz, $CDCl_3$): δ 9.28 (s, 1H), 9.10 (br_s, 1H), 8.62 (d, J = 7.8 Hz, 1H), 8.14 (d, J = 7.7 Hz, 1H), 7.70 (dd, J = 13.1, 2.3 Hz, 1H), 7.66 (d, J = 8.7 Hz, 1H), 7.59 (t, J = 7.7 Hz, 1H), 7.42 (d, J = 5.8 Hz, 1H), 7.27 (d, J = 6.0 Hz, 1H), 6.94 (t, J = 9.1 Hz, 1H), 6.77 (br_s, 1H), 5.63 (td, J = 22.9, 7.7 Hz, 1H), 4.24−4.11 (m, 8H), 1.24−1.20 (m, 12H). ^{31}P NMR (203 MHz, $CDCl_3$) δ 17.27 (s). ^{13}C NMR (126 MHz, $CDCl_3$): δ 168.4, 165.3, 158.5, 155.8 (t, J = 3.3 Hz), 152.2 (d, $^1J_{CF}$ = 244.1 Hz), 144.3 (d, J = 10.9 Hz), 138.0, 134.7, 132.6 (d, J = 9.4 Hz), 131.1, 130.2, 129.1, 126.8, 123.9, 117.9, 116.3 (d, J = 3.4 Hz), 115.5, 113.7 (d, J = 2.5 Hz), 109.7 (d, J = 22.6 Hz), 63.9−63.7 (m), 56.7, 46.9 (t, J = 147.9 Hz), 16.5−16.4 (m). MS [ESI$^+$] m/z: 681.3 [M + H$^+$]$^+$.

Inhibitor **11c** was isolated as a pale yellow solid. ^{1}H NMR (500 MHz, D_2O): δ 8.77 (s, 1H), 8.55 (d, J = 7.8 Hz, 1H), 8.03 (d, J = 7.8 Hz, 1H), 7.74 (t, J = 7.8 Hz, 1H), 7.64 (d, J = 5.9 Hz, 1H), 7.53−7.51 (m, 2H), 7.34 (d, J = 8.5 Hz, 1H), 7.23 (t, J = 9.1 Hz, 1H), 5.21 (t, J = 18.5 Hz, 1H), 3.95 (s, 3H). ^{31}P NMR (203 MHz, D_2O): δ 13.90 (s). ^{13}C NMR (126 MHz, D_2O): δ 168.8, 165.5, 159.5, 157.0, 151.3 (d, $^1J_{CF}$ = 242.1 Hz), 144.3 (d, J = 10.9 Hz), 138.1, 133.9, 132.0, 130.5 (d, J = 9.4 Hz), 129.3, 129.2, 126.8, 123.2, 118.7, 118.7 (d, J = 3.1 Hz), 115.8, 113.9 (d, J = 1.9 Hz), 111.0 (d, J = 21.8 Hz), 56.3, 49.0 (^{13}C-α observed by HSQC) . HSQC (^{1}H−^{13}C): ^{1}H at δ 5.19 correlates to ^{13}C-α at δ 49.0. HRMS [ESI$^+$] calculated for $C_{21}H_{17}O_8N_4FNa_3P_2S$ m/z, 634.991 40; found 634.991 64 [M + H]$^+$.

(((6-(3-Benzamidophenyl)thieno[2,3-*d*]pyrimidin-4-yl)-amino)methylene)bis(phosphonic acid) (12). Suzuki cross-coupling between intermediate tetraethyl (((6-bromothieno[2,3-*d*]pyrimidin-4-yl)amino)methylene)bis(phosphonate), which was previously reported,[40] and (3-benzamidophenyl)boronic acid (prepared as previously reported[62]) gave the tetraethyl (((6-(3-benzamidophenyl)thieno[2,3-*d*]pyrimidin-4-yl)amino)methylene)bis-(phosphonate), isolated as a light yellow solid (82%). ^{1}H NMR (400 MHz, DMSO-d_6): δ 10.43 (s, -NH), 8.71 (d, J = 9.7 Hz, -NH), 8.54 (s, 1H), 8.45 (s, 1H), 8.31 (d, J = 2.3 Hz, 1H), 8.03−7.99 (m, 2H), 7.77 (d, J = 7.5 Hz, 1H), 7.64−7.44 (m, 5H), 5.81 (td, J = 23.5, 9.1 Hz, 1H), 4.16−4.02 (m, 8H), 1.23−1.11 (m, 12H). ^{31}P NMR (162 MHz, DMSO-d_6) δ 16.88 (s). MS [ESI$^+$] m/z: 633.2 [M + H$^+$]$^+$.

Inhibitor **12** was isolated as a pale yellow solid. ^{1}H NMR (500 MHz, D_2O): δ 8.27 (s, 1H), 7.92−7.89 (m, 4H), 7.67−7.63 (m, 2H), 7.59−7.56 (m, 3H), 7.52 (t, J = 7.9 Hz, 1H). α-CH to the bisphosphonate overlaps with the solvent peak. ^{31}P NMR (203 MHz, D_2O): δ 13.53 (s). ^{13}C NMR (126 MHz, D_2O): δ 169.3, 163.2, 156.2, 153.5, 138.7, 137.9, 133.9, 133.5, 132.4, 129.9, 128.7, 127.3, 122.8, 121.8, 119.0, 118.6, 115.1, 50.8 (t, J = 125.7 Hz). HRMS [ESI$^+$] calculated for $C_{20}H_{16}N_4Na_3O_7P_2S$ m/z, 586.9903; found 586.9906 [M + H]$^+$.

2-(Methylthio)thieno[2,3-*d*]pyrimidin-4-amine (15). 2-Amino-5-methylthiophene-3-carbonitrile (**14**; 2.5 g, 20 mmol) was added to HCl (4 M in dioxane; 30.2 mL, 121 mmol), followed by methyl thiocyanate (1.4 mL, 20 mmol). The resulting suspension was heated to 70 °C in a sealed pressure tube for 36 h. The mixture was allowed to cool to rt, and the resulting green precipitate was collected by vacuum filtration. The solid was dissolved in EtOAc, washed with saturated aqueous $NaHCO_3$, and the aqueous phase was extracted further with EtOAc. The combined organic extracts were washed with brine, dried over Na_2SO_4, and concentrated in vacuo. Intermediate **15** was obtained as a light brown solid (2.52g, 63%) and was used in the next step without further purification. ^{1}H NMR (500 MHz, DMSO-d_6): δ 7.55 (br_s, 2H), 7.47 (d, J = 5.9 Hz, 1H), 7.36 (d, J = 5.9 Hz, 1H), 2.46 (s, 3H). ^{13}C NMR (126 MHz, DMSO-d_6): δ 167.5, 166.5, 158.3, 120.7, 120.2, 113.4, 13.8. MS [ESI$^+$] m/z: 198.0 [M + H$^+$]$^+$.

Tetraethyl (((2-(Methylthio)thieno[2,3-*d*]pyrimidin-4-yl)-amino)methylene)bis(phosphonate) (16). In a pressure vessel, diethyl phosphite (5.5 mL, 43 mmol) and triethyl orthoformate (1.7 mL, 10 mmol) were added to a solution of **15** (1.2 g, 6.1 mmol) in dry toluene (5.0 mL). The resulting mixture was heated at 130 °C for 40 h (monitored by TLC and/or LC−MS). The mixture was then cooled to rt and concentrated in vacuo. Crude product was purified by silica gel column chromatography. The product, intermediate **16**, eluted from the column with 10−20% MeOH in EtOAC and obtained as a light yellow solid (1.2 g, 41%). ^{1}H NMR (500 MHz, DMSO-d_6): δ 8.70 (d, J = 9.7 Hz, -NH), 7.97 (d, J = 6.0 Hz, 1H), 7.45 (d, J = 6.0 Hz, 1H), 5.70 (td, J = 23.6, 9.7 Hz, 1H), 4.14−4.02 (m, 8H), 2.50 (s, 3H), 1.21 (t, J = 7.1 Hz, 6H), 1.14 (t, J = 7.0 Hz, 6H). ^{31}P NMR (203 MHz, DMSO-d_6): δ 16.77 (s). ^{13}C NMR (126 MHz, DMSO-d_6): δ 167.3, 165.4, 155.12 (t, J = 4.1 Hz), 121.1, 120.1, 113.6, 62.9−62.7 (m), 44.4 (t, J = 147.3 Hz), 16.2−16.1 (m), 13.5. MS [ESI$^+$] m/z: 484.1 [M + H$^+$]$^+$.

General Protocol for the Synthesis of Intermediates 17a and 17b. This cross-coupling reaction was based on the literature with slight modifications.[60,61] Intermediate **16** (880 mg, 1.8 mmol), the arylboronic acid (4.6 mmol; obtained commercially or prepared using well established methods), CuTC (1.04 g, 5.5 mmol), and Pd(dppf)Cl_2·CH_2Cl_2 (150 mg, 0.18 mmol) were charged into an oven-dried round-bottom flask. The flask was evacuated and purged with Ar, followed by addition of dry dioxane (10.0 mL). The flask was sealed and heated at 50 °C for 4−16 h (under Ar balloon; monitored by TLC or LC−MS). The reaction mixture was cooled to rt, diluted with EtOAc, and filtered through Celite. The filtrate was collected and washed with 10% aqueous NH_4OH (thrice), followed by brine. The combined organic extracts were dried over Na_2SO_4 and concentrated

DOI: 10.1021/acs.jmedchem.8b00886
J. Med. Chem. 2018, 61, 6904−6917

in vacuo. Crude product was purified by silica gel column chromatography with a gradient from 25% EtOAc in hexanes to 100% EtOAc and then to 20% MeOH in EtOAc. Product typically eluted from the column with 10−20% MeOH in EtOAc and isolated in ∼80−85% yield.

Tetraethyl (((2-(3-Nitrophenyl)thieno[2,3-*d*]pyrimidin-4-yl)-amino)methylene)bis(phosphonate) (17a). Isolated as light brown solid. ^{1}H NMR (500 MHz, DMSO-d_6): δ 9.12 (t, J = 1.9 Hz, 1H), 8.85 (d, J = 9.6 Hz, -NH), 8.80 (d, J = 7.9 Hz, 1H), 8.35 (ddd, J = 8.2, 2.4, 0.9 Hz, 1H), 8.14 (d, J = 6.0 Hz, 1H), 7.84 (t, J = 8.0 Hz, 1H), 7.72 (d, J = 6.0 Hz, 1H), 5.99 (td, J = 23.5, 9.6 Hz, 1H), 4.23−4.02 (m, 8H), 1.20 (t, J = 7.0 Hz, 6H), 1.12 (t, J = 7.0 Hz, 6H). ^{31}P NMR (203 MHz, DMSO-d_6): δ 16.9. ^{13}C NMR (126 MHz, DMSO-d_6): δ 167.8, 156.5 (t, J = 4.0 Hz), 156.4, 148.7, 139.6, 134.1, 130.8, 125.3, 124.9, 122.4, 120.8, 116.4, 63.4−63.2 (m), 45.0 (t, J = 147.2 Hz), 16.7−16.6 (m). MS [ESI$^+$] m/z: 559.1 [M + H$^+$]$^+$.

Benzyl 3-(4-((Bis(diethoxyphosphoryl)methyl)amino)-thieno[2,3-*d*]pyrimidin-2-yl)benzoate (17b). Isolated as a light yellow solid. ^{1}H NMR (500 MHz, CD_3OD): δ 9.09 (s, 1H), 8.66 (d, J = 7.8 Hz, 1H), 8.14 (dd, J = 7.7, 1.1 Hz, 1H), 7.72 (d, J = 6.0 Hz, 1H), 7.64−7.58 (m, 1H), 7.55 (dd, J = 6.0, 1.5 Hz, 1H), 7.49 (d, J = 7.9 Hz, 2H), 7.41 (t, J = 7.5 Hz, 2H), 7.36−7.32 (m, 1H), 6.19 (t, J = 23.5 Hz, 1H), 5.42 (s, 2H), 4.24−4.18 (m, 8H), 1.27−1.21 (m, 12H). ^{31}P NMR (203 MHz, CD_3OD): δ 17.17 (s). ^{13}C NMR (126 MHz, CD_3OD): δ 169.5, 167.5, 159.4, 157.4 (t, J = 3.9 Hz), 139.7, 137.6, 133.6, 132.2, 131.8, 130.1, 129.9, 129.7, 129.3, 129.3, 125.3, 119.8, 117.1, 67.9, 65.2−65.1 (m), 45.5 (t, J = 150.0 Hz), 16.7−16.6 (m). MS [ESI$^-$] m/z: 648.3 [M − H$^+$]$^-$.

Tetraethyl (((2-(3-Aminophenyl)thieno[2,3-*d*]pyrimidin-4-yl)amino)methylene)bis(phosphonate) (18). In a pressure vessel containing intermediate **17a** (500 mg, 0.90 mmol) in EtOH (9.0 mL), $SnCl_2{\cdot}2H_2O$ (1.01 g, 4.5 mmol) was added, and the mixture was stirred at 80 °C for 2−3 h. The reaction mixture was cooled to rt and then slowly poured into sat. $NaHCO_3$ solution (9.0 mL). It was then extracted with EtOAc (3×), brine (once), dried over anhydrous $MgSO_4$, filtered, and concentrated in vacuo. Intermediate **18** was obtained as a light yellow solid (392 mg, 83% yield) and was used in the next step without further purification. ^{1}H NMR (500 MHz, DMSO-d_6): δ 8.52 (d, J = 9.7 Hz, 1H), 8.06 (d, J = 6.0 Hz, 1H), 7.64−7.62 (m, 1H), 7.58 (d, J = 6.0 Hz, 1H), 7.53 (d, J = 7.7 Hz, 1H), 7.14 (t, J = 7.8 Hz, 1H), 6.67 (dd, J = 7.9, 1.5 Hz, 1H), 6.01 (td, J = 23.5, 9.7 Hz, 1H), 5.22 (s, 2H), 4.15−4.05 (m, 8H), 1.16 (t, J = 7.0 Hz, 6H), 1.11 (t, J = 7.0 Hz, 6H). ^{31}P NMR (203 MHz, DMSO-d_6): δ 17.18 (s). MS [ESI$^+$] m/z: 529.1 [M + H$^+$]$^+$.

3-(4-((Bis(diethoxyphosphoryl)methyl)amino)thieno[2,3-*d*]-pyrimidin-2-yl)benzoic Acid (19). A solution of intermediate **17b** (271 mg, 0.42 mmol) in neat TFA (4.6 mL) was stirred at 80 °C for 14 h (monitored by TLC). TFA was then removed by evaporation in vacuo, and the residue was dissolved in DCM, and the solvent was evaporated again under reduced pressure (done at least twice). Crude product was purified by silica gel column chromatography using a gradient of 50% EtOAc in hexanes to 100% EtOAc and then to 15% MeOH in EtOAc. Product was isolated as a light brown solid (quantitative yield). ^{1}H NMR (400 MHz, $CDCl_3$ with ∼0.1% CD_3OD): δ 9.20 (s, 1H), 8.70 (d, J = 7.9 Hz, 1H), 8.19 (d, J = 7.7 Hz, 1H), 7.70 (d, J = 6.0 Hz, 1H), 7.59 (t, J = 7.8 Hz, 1H), 7.40 (d, J = 6.0 Hz, 1H), 6.08 (t, J = 22.2 Hz, 1H), 4.29−4.18 (m, 8H), 1.29 (t, J = 7.0 Hz, 6H), 1.20 (t, J = 7.0 Hz, 6H). ^{31}P NMR (203 MHz, $CDCl_3$): δ 17.50 (s). ^{13}C NMR (126 MHz, $CDCl_3$ with ∼0.1% CD_3OD) δ 169.2, 168.3, 158.4, 155.8, 138.4, 132.7, 131.5, 129.8, 128.6, 123.8, 118.8, 115.9, 115.8, 64.2 (br), 44.1 (t, J = 147.0 Hz, 1H), 16.2 (br). MS [ESI$^+$] m/z: 558.1 [M + H$^+$]$^+$.

■ ASSOCIATED CONTENT

Supporting Information

The Supporting Information is available free of charge on the ACS Publications Web site at DOI:10.1021/acs.jmedchem- . (CSV). The Supporting Information is available free of charge on the ACS Publications website at DOI: 10.1021/acs.jmedchem.8b00886.

Experimental procedures for (a) the expression, purification, and in vitro assay of recombinant hGGPPS, (b) creation of the dimeric Y246D mutant of hGGPPS and crystallographic studies with inhibitor **10d**, (c) cell culture and viability assays for MM cell lines, (d) cell culture for various other cancer cell lines (non-MM), (e) determination of cancer cell viability for non-MM cancer cells, (f) annexin-V apoptosis assays, (g) Western blot analysis, (h) XBP1 mRNA splicing, (i) metabolic stability, (j) in vivo experiments with MM mouse diseases model, (k) serum protein electrophoresis (SPEP), (l) isolation of peripheral blood mononuclear cells (PBMCs), (m) DSF studies; Figures S1−S8; Tables S1−S3; ^{1}H, ^{31}C, ^{31}P NMR spectra and HPLC chromatograms for inhibitors **10a−d** and **11a−c** (PDF)

Molecular formula strings and biological data (CSV)

Accession Codes

The PDB accession codes for the X-ray structures of the dimeric hGGPPS Y245D mutant and the structure of **10d** bound to this mutant are 6C56 and 6C57, respectively. Authors will release the atomic coordinates and experimental data upon article publication.

■ AUTHOR INFORMATION

Corresponding Authors

*M.S.: e-mail, Michael.sebag@mcgill.ca; phone, + 514-843-1558.

*Y.S.T.: e-mail, Youla.tsantrizos@mcgill.ca; phone, +514-398-3638.

ORCID

Jaeok Park: 0000-0002-8180-3950

Youla S. Tsantrizos: 0000-0002-6231-7498

Author Contributions

$^{\perp}$C.M.L., D.D.W., and M.G.P contributed equally. Author contributions are the following: conceptualization and coordination of project (Y.S.T.); design of hematology, cellular, and in vivo studies (M.S.); library synthesis and in vitro evaluation of inhibitors (C.M.L.); biology experiments (D.D.W., M.G.P., X.F.H., J.P); cloning, protein production, and crystallography (J.P., V.T., A.M.B.); DSF and bone affinity studies (F.V.)

Notes

The authors declare no competing financial interest.

■ ACKNOWLEDGMENTS

Financial support for this work was provided by the Canadian Institute of Health Research (CIHR) and Fonds Québécois de la Research sur la Nature et les Technologies (FRQNT) research grants to A.M.B., M.S. and Y.S.T. Data in Figure 5,b was generated as part of the Multiple Myeloma Research Foundation Personalized Medicine Initiatives (https://research.themmrf.org and www.themmrf.org). The authors thank Opher Gileadi of the Structural Genomics Consortium (SGC) at the University of Oxford for providing the wild-type human GGPPS pNIC28-Bsa4 vector.

■ ABBREVIATIONS USED

hFPPS, human farnesyl pyrophosphate synthase; hGGPPS, human geranylgeranyl pyrophosphate synthase; FTase, farnesyl

DOI: 10.1021/acs.jmedchem.8b00886
J. Med. Chem. 2018, 61, 6904−6917

transferase; GGTase I and II, geranylgeranyl transferase I and II; GTPase, small GTP-binding protein; MM, multiple myeloma; MLM, mouse liver microsome; RLM, rat liver microsome; HLM, huma liver microsome; SPEP, serum protein electrophoresis; PBMC, peripheral blood mononuclear cell; DSF, differential scanning fluorimetry; PBS, phosphate buffered saline; ip, intraperitoneal injection

REFERENCES

(1) Nguyen, U. T. T.; Guo, Z.; Delon, C.; Wu, Y.; Deraeve, C.; Fränzel, B.; Bon, R. S.; Blankenfeldt, W.; Goody, R. S.; Waldmann, H.; Wolters, D.; Alexandrov, K. Analysis of the eukaryotic prenylome by isoprenoid affinity tagging *Nature*. *Nat. Chem. Biol.* **2009**, *5*, 227−235.

(2) Kho, Y.; Kim, S. C.; Jiang, C.; Barma, D.; Kwon, S. W.; Cheng, J.; Jaunbergs, J.; Weinbaum, C.; Tamanoi, F.; Falck, J.; Zhao, Y. A tagging-via-substrate technology for detection and proteomics of farnesylated proteins. *Proc. Natl. Acad. Sci. U. S. A.* **2004**, *101*, 12479−12484.

(3) Stark, J. L.; Mehla, K.; Chaika, N.; Acton, T. B.; Xiao, R.; Singh, P. K.; Montelione, G. T.; Powers, R. Structure and function of human DnaJ homologues subfamily A member 1 (DNAJA1) and its relationship to pancreatic cancer. *Biochemistry* **2014**, *53*, 1360−1372.

(4) Kampinga, H. H.; Craig, E. A. The HSP70 chaperone machinery J proteins as drivers of functional specificity. *Nat. Rev. Mol. Cell Biol.* **2010**, *11*, 579−592.

(5) Young, S. G.; Fong, L. G.; Michaelis, S. Prelamin A, Zmpste24, misshapen cell nuclei, and progeria − new evidence suggesting that protein farnesylation could be important for diseases pathogenesis. *J. Lipid Res.* **2005**, *46*, 2531−2558.

(6) Takai, Y.; Sasaki, T.; Matozaki, T. Small GTP-binding roteins. *Physiol. Rev.* **2001**, *81*, 153−208.

(7) Mullen, P. J.; Yu, R.; Longo, J.; Archer, M. C.; Penn, L. Z. The interplay between cell signaling and the mevalonate pathway in cancer. *Nat. Rev. Cancer* **2016**, *16*, 718−731.

(8) Clendening, J. W.; Pandyra, A.; Boutros, P. C.; Ghamrasni, S. E.; Khosravi, F.; Trentin, G. A.; Martirosyan, A.; Hakem, A.; Hakem, R.; Jurisica, I.; Penn, L. Z. Dysregulation of the mevalonate pathway promotes transformation. *Proc. Natl. Acad. Sci. U. S. A.* **2010**, *107*, 15051−15056.

(9) Sorrentino, G.; Ruggeri, N.; Specchia, V.; Cordenonsi, M.; Mano, M.; Dupont, S.; Manfrin, A.; Ingallina, E.; Sommaggio, R.; Piazza, S.; Rosato, A.; Piccolo, S.; Del Sal, G. Metabolic control of YAP and TAZ by the mevalonate pathway. *Nat. Cell Biol.* **2014**, *16*, 357−366.

(10) Nielsen, S. F.; Nordestgaard, B. G.; Bojesen, S. E. Statin use and reduced cancer-related mortality. *N. Engl. J. Med.* **2012**, *367*, 1792−1802.

(11) Garwood, E. R.; Kumar, A. S.; Baehner, F. L.; Moore, D. H.; Au, A.; Hylton, N.; Flowers, C. I.; Garber, J.; Lesnikoski, B. A.; Hwang, E. S.; Olopade, O.; Port, E. R.; Campbell, M.; Esserman, L. J. Fluvastatin reduces proliferation and increases apoptosis in women with high grade breast cancer. *Breast Cancer Res. Treat.* **2010**, *119*, 137−144.

(12) Kubatka, P.; Kruzliak, P.; Rotrekl, V.; Jelinkova, S.; Mladosievicova, B. Statins in oncological research: from experimental studies to clinical practice. *Crit. Rev. Oncol. Hematol.* **2014**, *92*, 296−311.

(13) Sanfilippo, K. M.; Keller, J.; Gage, B. F.; Luo, S.; Wang, T.-F.; Moskowitz, G.; Gumbel, J.; Blue, B.; O'Brian, K.; Carson, K. Statins are associated with reduced mortality in multiple myeloma. *J. Clin. Oncol.* **2016**, *34*, 4008−4014.

(14) Dunford, J. E. Molecular targets of the nitrogen containing bisphosphonates: The molecular pharmacology of prenyl synthase inhibition. *Curr. Pharm. Des.* **2010**, *16*, 2961−2969.

(15) Ebetino, F. H.; Hogan, A.-M.; Sun, S.; Tsoumpra, M. K.; Duan, X.; Triffitt, J. T.; Kwaasi, A. A.; Dunford, J. E.; Barnett, B. L.; Oppermann, U.; Lundy, M. W.; Boyde, A.; Kashemirov, B. A.; McKenna, C. E.; Russell, R. G. The relationship between the chemistry and biological activity of the bisphosphonates. *Bone* **2011**, *49*, 20−33.

(16) Coleman, R. E.; Marshall, H.; Cameron, D.; Dodwell, D.; Burkinshaw, R.; Keane, M.; Gil, M.; Houston, S. J.; Grieve, R. J.; Barrett-Lee, P. J.; Ritchie, D.; Pugh, J.; Gaunt, C.; Rea, U.; Peterson, J.; Davies, C.; Hiley, V.; Gregory, W.; Bell, R. Breast-cancer adjuvant therapy with zoledronic acid. *N. Engl. J. Med.* **2011**, *365*, 1396−1405.

(17) Gnant, M.; Mlineritsch, B.; Stoeger, H.; Luschin-Ebengreuth, G.; Heck, D.; Menzel, C.; Jakesz, R.; Seifert, M.; Hubalek, M.; Pristauz, G.; Bauernhofer, T.; Eidtmann, H.; Eiermann, W.; Steger, G.; Kwasny, W.; Dubsky, P.; Hochreiner, G.; Forsthuber, E. P.; Fesl, C.; Greil, R. Adjuvant endocrine therapy plus zoledronic acid in premenopausal women with early-stage breast cancer: 62-month follow-up from the ABCSG-12 randomised trial. *Lancet Oncol.* **2011**, *12*, 631−641.

(18) Gnant, M.; Mlineritsch, B.; Schippinger, W.; Luschin-Ebengreuth, G.; Pöstlberger, S.; Menzel, C.; Jakesz, R.; Seifert, M.; Hubalek, M.; Bjelic-Radisic, V.; Samonigg, H.; Tausch, C.; Eidtmann, H.; Steger, G.; Kwasny, W.; Dubsky, P.; Fridrik, M.; Fitzal, F.; Stierer, M.; Rücklinger, E.; Greil, R. Endocrine therapy plus zoledronic acid in premenopaisal breast cancer. *N. Engl. J. Med.* **2009**, *360*, 679−691.

(19) Coleman, R. E.; de Boer, R.; Eidtmann, H.; Llombart, A.; Davidson, N.; Neven, P.; von Minckwitz, G.; Sleeboom, H. P.; Forbes, J.; Barrios, C.; Frassoldati, A.; Campbell, I.; Paija, O.; Martin, N.; Modi, A.; Bundred, N. Zoledronic acid (zoledronate) for post-menopausal women with early breast cancer receiving adjuvant letrozole (ZO-FAST study): 60-months results. *Ann. Oncol.* **2013**, *24*, 398−405.

(20) Morgan, G. J.; Davies, F. E.; Gregory, W. M.; Cocks, K.; Bell, S. E.; Szubert, A. J.; Navarro-Coy, N.; Drayson, M. T.; Owen, R. G.; Feyler, S.; Ashcroft, A. J.; Ross, F.; Byrne, J.; Roddie, H.; Rudin, C.; Cook, G.; Jackson, G. H.; Child, J. A. First-line treatment with zoledronic acid as compared with clodronic acid in multiple myeloma (MRC Myeloma IX): a randomized controlled trial. *Lancet* **2010**, *376*, 1989−1999.

(21) Morgan, G. J.; Davies, F. E.; Gregory, W. M.; Szubert, A. J.; Bell, S. E.; Drayson, M. T.; Owen, R. G.; Ashcroft, A. J.; Jackson, G. H.; Child, J. A. Effects of induction and maintenance plus long-term bisphosphonates on bone disease in patients with multiple myeloma: the Medical Research Council Myeloma IX Trial. *Blood* **2012**, *119*, 5374−5383.

(22) Skerjanec, A.; Berenson, J.; Hsu, C.; Major, P.; Miller, W. H., Jr.; Ravera, C.; Schran, H.; Seaman, J.; Waldmeier, F. The pharmacokinetics and pharmacodynamics of zoledronic acid in cancer patients with varying degrees of renal function. *J. Clin. Pharmacol.* **2003**, *43*, 154−162.

(23) Weiss, H. M.; Pfaar, U.; Schweitzer, A.; Wiegand, H.; Skerjanec, A.; Schran, H. Biodistribution and plasma protein binding of zoledronic acid. *Drug Metab. Dispos.* **2008**, *36*, 2043−2049.

(24) Jahnke, W.; Rondeau, J.-M.; Cotesta, S.; Marzinzik, A.; Pellé, X.; Geiser, M.; Strauss, A.; Götte, M.; Bitsch, F.; Hemmig, R.; Henry, C.; Lehmann, S.; Glickman, J. F.; Roddy, T. P.; Stout, S. J.; Green, J. R. Allosteric non-bisphosphonate FPPS inhibitors identified by fragment-based discovery. *Nat. Chem. Biol.* **2010**, *6*, 660−666.

(25) De Schutter, J. W.; Park, J.; Leung, C. Y.; Gormley, P.; Lin, Y. S.; Hu, Z.; Berghuis, A. M.; Poirier, J.; Tsantrizos, Y. S. Multistage screening reveals chameleon ligands of human farnesyl pyrophosphate synthase: Implications to drug discovery for neurodegenerative diseases. *J. Med. Chem.* **2014**, *57*, 5764−5776.

(26) Marzinzik, A. L.; Amstutz, R.; Bold, G.; Bourgier, E.; Cotesta, S.; Glickman, J. F.; Götte, M.; Henry, C.; Lehmann, S.; Hartwieg, J. C. D.; Ofner, S.; Pellé, X.; Roddy, T. P.; Rondeau, M.; Stauffer, F.; Stout, S. J.; Widmer, A.; Zimmermann, J.; Zoller, T.; Jahnke, W. Discovery of novel allostetic non-bisphosphonate inhibitors of farnesyl pyrophosphate synthase by integrated lead finding. *ChemMedChem* **2015**, *10*, 1884−1891.

(27) Park, J.; Leung, C. Y.; Matralis, A. N.; Lacbay, C. M.; Tsakos, M.; Fernandez De Troconiz, G.; Berghuis, A. M.; Tsantrizos, Y. S.

DOI: 10.1021/acs.jmedchem.8b00886
J. Med. Chem. 2018, 61, 6904−6917

Pharmacophore mapping of thienopyrimidine-based monophosphonate (ThP-MP) inhibitors of the human farnesyl pyrophosphate synthase. *J. Med. Chem.* **2017**, *60*, 2119−2134.
(28) Lobell, R. B.; Liu, D.; Buser, C. A.; Davide, J. P.; DePuy, E.; Hamilton, K.; Koblan, K. S.; Lee, Y.; Mosser, S.; Motzel, S. L.; Abbruzzese, J. L.; Fuchs, C. S.; Rowinsky, E. K.; Rubin, E. H.; Sharma, S.; Deutsch, P. J.; Mazina, K. E.; Morrison, B. W.; Wildonger, L.; Yao, S.-L.; Kohl, N. E. Preclinical and clinical pharmacodynamic assessment of L-778, 123, a dual inhibitor of farnesyl:protein transfgerase and geranylgeranyl:ptotein tansferase type-I. *Mol. Cancer Ther* **2002**, *1*, 747−758.
(29) Martin, N. E.; Brunner, T. B.; Kiel, K. D.; DeLaney, T. F.; Regine, W. F.; Mohiuddin, M.; Rosato, E. F.; Haller, D. G.; Stevenson, J. P.; Smith, D.; Pramanik, B.; Tepper, J.; Tanaka, W. K.; Morrison, B.; Deutsch, P.; Gupta, A. K.; Muschel, R. J.; McKenna, G.; Bernhard, E. J.; Hahn, S. M. A phase I trial of the dual farnesyltransferase and geranylgeranyltransferase inhibitor L-778,123 and radiotherapy for locally advanced pancreatic cancer. *Clin. Cancer Res.* **2004**, *10*, 5447−5454.
(30) Yokoyama, K.; Zimmerman, K.; Scholten, J.; Gelb, M. H. Differential prenyl pyrophosphate binding to mammalian protein geranylgeranyltransferase-I and protein farnesyltransferase and its consequence on the specificity of protein prenylation. *J. Biol. Chem.* **1997**, *272*, 3944−3952.
(31) Rowinsky, E. K. Lately, it occurs to me what a long, strange trip it's been for the farnesyltransferase inhibitors. *J. Clin. Oncol.* **2006**, *24*, 2981−2984.
(32) Zhang, Y.; Cao, R.; Yin, F.; Lin, F.-Y.; Wang, H.; Krysiak, K.; No, J.-H.; Mukkamala, D.; Houlihan, K.; Li, J.; Morita, C. T.; Oldfield, E. Lipophilic pyridinium bisphosphonates: Potent $\gamma\delta$ T cell stimulators. *Angew. Chem., Int. Ed.* **2010**, *49*, 1136−1138.
(33) Zhang, Y.; Cao, R.; Yin, F.; Hudock, M. P.; Guo, R.-T.; Krysiak, K.; Mukherjee, S.; Gao, Y.-G.; Robinson, H.; Song, Y.; No, J. H.; Bergan, K.; Leon, A.; Cass, L.; Goddard, A.; Chang, T.-K.; Lin, F.-Y.; Van Beek, E.; Papapoulos, S.; Wang, A.H.-J.; Kubo, T.; Ochi, M.; Mukkamala, D.; Oldfield, E. Lipophilic bisphosphonates as dual farnesyl/geranylgeranyl diphosphate synthase inhibitors: An X-ray and NMR investigation. *J. Am. Chem. Soc.* **2009**, *131*, 5153−5162.
(34) Shull, L. W.; Wiemer, A. J.; Hohl, R. J.; Wiemer, D. F. Synthesis and biological activity of isoprenoid bisphosphonates. *Bioorg. Med. Chem.* **2006**, *14*, 4130−4136.
(35) Wills, V. S.; Allen, C.; Holstein, S. A.; Wiemer, D. F. Potent triazole bisphosphonate inhibitor of geranylgeranyl diphosphate synthase. *ACS Med. Chem. Lett.* **2015**, *6*, 1195−1198.
(36) Wills, V. S.; Metzger, J. I.; Allen, C.; Varney, M. L.; Wiemer, D. F.; Holstein, S. A. Bishomoisoprenoid triazole bisphosphonates as inhibitors of geranylgeranyl diphosphate synthase. *Bioorg. Med. Chem.* **2017**, *25*, 2437−2444.
(37) Guenther, A.; Gordon, S.; Tiemann, M.; Burger, R.; Bakker, F.; Green, J. R.; Baum, W.; Roelofs, A. J.; Rogers, M. J.; Gramatzki, M. The bisphosphonate zoledronic acid has antimyeloma activity in vivo by inhibition of protein prenylation. *Int. J. Cancer* **2010**, *126*, 239−246.
(38) Leung, C.-Y.; Langille, A. M.; Mancuso, J.; Tsantrizos, Y. S. Discovery of thienopyrimidine-based inhibitors of the human farnesyl pyrophosphate synthase − Parallel synthesis of analogs via a thrimethylsilyl ylidene intermediate. *Bioorg. Med. Chem.* **2013**, *21*, 2229−2240.
(39) Kavanagh, K. L.; Dunford, J. E.; Bunkoczi, G.; Russell, R. G. G.; Oppermann, U. J. The crystal structure of human geranylgeranyl pyrophosphate synthase reveals a novel hexameric arrangement and inhibitory product binding. *J. Biol. Chem.* **2006**, *281*, 22004−22012.
(40) Leung, C. Y.; Park, J.; De Schutter, J. W.; Sebag, M.; Berghuis, A. M.; Tsantrizos, Y. S. Thienopyrimidine bisphosphomates (ThPBP) inhibitors of the human farnesyl pyrophosphate synthase: Optimization and characterization of the mode of inhibition. *J. Med. Chem.* **2013**, *56*, 7939−7950.
(41) For details on the characterization of MM cells lines, refer to Keats lab Web site: http://www.keatslab.org/projects/mm-cell-line-characterization/cell-line-characterization-status.
(42) Hideshima, T.; Cottini, F.; Nozawa, Y.; Seo, H.-S.; Ohguchi, H.; Samur, M. K.; Cirstea, D.; Mimura, N.; Iwasawa, Y.; Richardson, P. G.; Munshi, N. C.; Chauhan, D.; Massefski, W.; Utsugi, T.; Dhe-Paganon, S.; Anderson, K. C. p53-Related protein kinase confers poor prognosis and represents a novel therapeutic target in multiple myeloma. *Blood* **2017**, *129*, 1308−1319.
(43) Shipman, C. M.; Croucher, P. I.; Russel, R. G. G.; Helfrich, M. H.; Rogers, M. J. The bisphosphnate incadronate (YM175) causes apoptosis of human myeloma cells in vitro by inhibiting the mevalonate pathway. *Cancer Res.* **1998**, *58*, 5294−5297.
(44) Jagdev, S. P.; Coleman, R. E.; Shipman, C. M.; Rostami-H, A.; Croucher, P. I. The bisphosphonate, zoledronic acid, induces apoptosis of breast cancer cells: evidence for synergy with paclitaxel. *Br. J. Cancer* **2001**, *84*, 1126−1134.
(45) Fujita, M.; Tohi, M.; Sawada, K.; Yamamoto, Y.; Nakamura, T.; Yagami, T.; Yamamori, M.; Okamura, N. Involvement of the mevalonate pathway in the antiproliferative effects of zoledronate on ACHN renal cell carcinoma cells. *Oncol. Rep.* **2012**, *27*, 1371−1376.
(46) Okamoto, S.; Jiang, Y.; Kawamura, K.; Shingyoji, M.; Tada, Y.; Sekine, I.; Takiguchi, Y.; Tatsumi, K.; Kobayashi, H.; Shimada, H.; Hiroshima, K.; Tagawa, M. Zoledronic acid induces apoptosis and S-phase arrest in mesothelioma through inhibiting Rab family proteins and topoisomerase II actions. *Cell Death Dis.* **2014**, *5*, e1517.
(47) Van de Donk, N. W. C. J.; Lokhorst, H. M.; Nijhuis, E. H. J.; Kamphuis, M. M. J.; Bloem, A. C. Geranylgeranylated proteins are involved in the regulation of myeloma cell growth. *Clin. Cancer Res.* **2005**, *11*, 429−439.
(48) Holstein, S. A.; Hohl, R. J. Isoprenoid biosynthetic pathway inhibition disrupts monoclonal protein secretion and induces the unfolded protein response pathway in multiple myeloma cells. *Leuk. Res.* **2011**, *35*, 551−559.
(49) The Cancer Cell Line Encyclopedia and Genomics of Drug Sensitivity in Cancer Consortium.. Pharmacogenomic agreement between two cancer cell line data sets. *Nature* **2015**, *528*, 84−87.
(50) Keats, J. J.; Craig, D. W.; Liang, W.; Venkata, Y.; Kurdoglu, A.; Aldrich, J.; Auclair, D.; Allen, K.; Harrison, B.; Jewell, S.; Kidd, P. G.; Correll, M.; Jagannath, S.; Siegel, D. S.; Vij, R.; Orloff, G.; Zimmerman, T. M.; Mmrf CoMMpass Network; Capone, W.; Carpten, J.; Lonial, S. Interim analysis of the mmrf commpass trial, a longitudinal study in multiple myeloma relating clinical outcomes to genomic and immunophenotypic profiles. *Blood* **2013**, *122*, 532.
(51) Lonial, S.; Yellapantula, V. D.; Liang, W.; Kurdoglu, A.; Aldrich, J.; Legendre, C. M.; Stephenson, K.; Adkins, J.; McDonald, J.; Helland, A.; Russell, M.; Christofferson, A.; Cuyugan, L.; Rohrer, D.; Blanski, A.; Hodges, M.; Mmrf CoMMpass Network; Derome, M.; Auclair, D.; Kidd, P. G.; Jewell, S.; Craig, D.; Carpten, J.; Keats, J. J. Interim analysis of the Mmrf Commpass Trial: identification of novel rearrangements potentially associated with disease initiation and progression. *Blood* **2014**, *124*, 722.
(52) Keats, J. J.; Speyer, G.; Christofferson, A.; Legendre, C.; Aldrich, J.; Russell, M.; Cuyugan, L.; Adkins, J.; Blanski, A.; Hodges, M.; Rohrer, D.; Jagannath, S.; Vij, R.; Orloff, G.; Zimmerman, T.; Niesvizky, R.; Liles, D.; Fay, J. W.; Wolf, J. L.; Rifkin, R. M.; Gutierrez, N. C.; Mmrf CoMMpass Network; Yesil, J.; Derome, M.; Kim, S.; Liang, W.; Kidd, P. G.; Jewell, S.; Carpten, J. D.; Auclair, D.; Lonial, S. Molecular predictors of outcome and drug response in multiple myeloma: An interim analysis of the Mmrf CoMMpass study. *Blood* **2016**, *128*, 194.
(53) Van Beek, E. R.; Löwik, C. W. G. M.; Papapoulos, S. E. Bisphosphonates suppress bone resorption by a direct effect on early osteoclast precursors without affecting the osteoclastogenic capacity of osteogenic cells: the role of protein geranylgeranylation in the action of nitrogen-containing bisphosphonates on osteoclast precursors. *Bone* **2002**, *30*, 64−70.

DOI: 10.1021/acs.jmedchem.8b00886
J. Med. Chem. 2018, 61, 6904−6917

(54) Jahnke, W.; Henry, C. An *in vitro* assay to measure targeted drug delivery to bone mineral. *ChemMedChem* **2010**, *5*, 770−776.
(55) Chesi, M.; Matthews, G. M.; Garbitt, V. M.; Palmer, S. E.; Shortt, J.; Lefebure, M.; Stewart, A. K.; Johnstone, R. W.; Bergsagel, P. L. Drug response in a genetically engineered mouse model of multiple myeloma is predictive of clinical efficacy. *Blood* **2012**, *120*, 376−385.
(56) Gomez-Palou, M.; Fang, H.; Kremer, R.; Sebag, M. A transgenic model of multiple myeloma bone disease shows profound mesenchymal stem cell impairment. *Blood* **2013**, *112*, 130.
(57) Vieira, P.; Rajewsky, K. The half-lives of serum immunoglobulins in adult mice. *Eur. J. Immunol.* **1988**, *18*, 313−316.
(58) For a recent review on the biology/physiology and clinical characteristics of multiply myeloma, refer to the following: Bianchi, G.; Munshi, N. Pathogenesis beyond the cancer clone(s) in multiple myeloma. *Blood* **2015**, *125*, 3049−3058.
(59) Coxon, F. P.; Helfrich, M. H.; van't Hof, R.; Sebti, S.; Ralston, S. H.; Hamilton, A.; Rogers, M. J. Protein geranylgeranylation is required for osteoclast formation, function and survival: Inhibition by bisphosphonates and GGTI-298. *J. Bone Miner. Res.* **2000**, *15*, 1467−1476.
(60) Barbay, J. K.; Chakravarty, D.; Shook, B. C.; Wang, A. Methylene Amines of Thieno[2,3-*d*]pyrimidine and Their Use as Adenosine a2a Receptor Antagonists. WO2010/045006 A1, April 22, 2010.
(61) Liebeskind, L. S.; Srogl, J. Heteroaromatic thioether-boronic acid cross-coupling under neutral reaction conditions. *Org. Lett.* **2002**, *4*, 979−981.
(62) Wetzel, M.; Marchais-Oberwinkler, S.; Hartmann, R.-W. 17b-HSD2 inhibitors for the treatment of osteoporosis: Identification of a promising scaffold. *Bioorg. Med. Chem.* **2011**, *19*, 807−815.

DOI: 10.1021/acs.jmedchem.8b00886
J. Med. Chem. 2018, 61, 6904−6917